

2019-01-01

## **Petrophysical, Geostatistical and Geo-spatial Analysis of Round Top Mountain Rhyolite (Hudspeth County, west Texas, USA)**

Lorraine Marie Negron  
*University of Texas at El Paso*

Follow this and additional works at: [https://digitalcommons.utep.edu/open\\_etd](https://digitalcommons.utep.edu/open_etd)



Part of the [Geology Commons](#)

---

### **Recommended Citation**

Negron, Lorraine Marie, "Petrophysical, Geostatistical and Geo-spatial Analysis of Round Top Mountain Rhyolite (Hudspeth County, west Texas, USA)" (2019). *Open Access Theses & Dissertations*. 2881.  
[https://digitalcommons.utep.edu/open\\_etd/2881](https://digitalcommons.utep.edu/open_etd/2881)

This is brought to you for free and open access by ScholarWorks@UTEP. It has been accepted for inclusion in Open Access Theses & Dissertations by an authorized administrator of ScholarWorks@UTEP. For more information, please contact [lweber@utep.edu](mailto:lweber@utep.edu).

PETROPHYSICAL, GEOSTATISTICAL AND GEO-SPATIAL ANALYSIS OF  
ROUND TOP MOUNTAIN RHYOLITE (HUDSPETH COUNTY,  
WEST TEXAS, USA)

LORRAINE MARIE NEGRÓN

Doctoral Program in Geological Sciences

APPROVED:

---

Nicholas E. Pingitore, Ph.D., Chair

---

Laura F. Serpa, Ph.D

---

Richard S Jarvis, Ph.D

---

Aaron A. Velasco, Ph.D

---

Maria Amaya, Ph.D

---

Stephen L. Crites Ph.D.  
Dean of the Graduate School

Copyright ©

by

Lorraine M. Negrón

2019

## **Dedication**

**I WOULD LIKE TO DEDICATE THIS ACCOMPLISHMENT FIRST AND FOREMOST TO MY FAMILY. TO MY PARENTS ANGEL NEGRÓN M.D. AND LEDYS NEGRÓN AS WELL AS MY SIBLINGS MARIA NEGRÓN-KNEIB AND RICARDO NEGRÓN M.D. I WOULD ALSO LIKE TO THANK GRANDMA ANNIE FOR ALWAYS TELLING ME THE HARD THINGS TO HEAR THAT FORCED ME TO BETTER MYSELF EACH AND EVERYDAY. TO MY NEPHEW, TOMÁS, AND MY NIECE, ADRIANA, WHO'S SMILES, PHOTOS AND VIDEOS MADE THE HARDEST DAYS BEARABLE. KNOW THAT YOU CAN ACHIEVE GREAT THINGS WITH HARD WORK, LOVE FROM YOUR FAMILY AND BELIEF IN YOURSELF.**

PETROPHYSICAL, GEOSTATISTICAL AND GEO-SPATIAL ANALYSIS OF  
ROUND TOP MOUNTAIN RHYOLITE (HUDSPETH COUNTY,  
WEST TEXAS, USA)

by

LORRAINE MARIE NEGRÓN, B.S.

DISSERTATION

Presented to the Faculty of the Graduate School of  
The University of Texas at El Paso  
in Partial Fulfillment  
of the Requirements  
for the Degree of

DOCTOR OF PHILOSOPHY

Department of Geological Sciences  
THE UNIVERSITY OF TEXAS AT EL PASO

December 2019

## **Acknowledgements**

I would like to acknowledge my graduate advisor, Dr. Pingitore who has been a father figure to me while I was far from home. He challenged me, stretched my capabilities beyond my own vision, and was tough on me that built confidence and character. To my friends who were always ready with motivational speeches that kept this endeavor within reach. To my colleagues who helped me study for qualifying exams, presentation practice, and multiple manuscript edits. To the many professors in the Geology department at the University of Texas at El Paso for always knowing my potential and encouraging me to surpass it.

# Table of Contents

Acknowledgements.....	v
Table of Contents.....	vi
List of Tables .....	ix
List of Figures.....	x
Chapter 1: Introduction.....	1
Chapter 2: Porosity and Permeability of Round Top Mountain Rhyolite (Texas, USA) Favor Coarse Crush Size for Rare Earth Element Heap Leach.....	2
2.1 ABSTRACT.....	2
2.2 INTRODUCTION .....	3
2.3 MATERIALS AND METHODS.....	7
2.3.1 Rhyolite Samples .....	7
2.3.2 Porosity Measurements.....	8
2.3.3 Permeability Measurements.....	10
2.4 RESULTS .....	12
2.4.1 Pre-Acid-Leach Porosity.....	12
2.4.2 Post-Acid-Leach Porosity .....	14
2.4.3 Permeability .....	16
2.5 DISCUSSION .....	18
2.5.1 Significance of Round Top Rhyolite Porosity and Permeability.....	18
2.5.2 Heap Leach Efficiency: Pink vs. Gray Rhyolite Varieties .....	19
2.5.3 Ionic Diffusion: Rate Limiting Step for Round Top Heap Leach .....	20
2.5.4 Unconventional Opportunity to Heap Leach Coarse-Crushed Crystalline Rock.....	21
2.6 CONCLUSIONS.....	22
ACKNOWLEDGEMENTS.....	23
References.....	23
Chapter 3: ArcGIS™ and Principal Component Analysis of Probe Data to Micro-map Minerals in Round Top Rare Earth Deposit .....	28
3.1 ABSTRACT.....	28

3.2 INTRODUCTION .....	29
3.2.1 Background .....	31
3.3 SAMPLE SOURCE AND PREPARATION .....	31
3.3.1 Sample collection .....	31
3.3.2 Thin section preparation .....	32
3.3.3 Electron probe microanalysis .....	32
3.3.4 X-ray Map Analyzer .....	34
3.3.5 Principal Component Analysis .....	34
3.3.6 ArcGIS™ .....	35
3.3.7 Integrating EPMA, XRMA-PCA, and ArcGIS™ .....	35
3.4 RESULTS AND DISCUSSION .....	35
3.4.1 Principal Component Analyses .....	35
3.4.2 Principal Components: Major Minerals .....	39
3.4.2.1 Potassium Feldspar .....	39
3.4.2.2 Quartz .....	40
3.4.2.3 Albite .....	40
3.4.3 Principal Components: Minor and Accessory Minerals .....	42
3.4.3.1 Annite mica .....	42
3.4.3.2 Magnetite .....	43
3.4.3.3 Yttrifluorite .....	43
3.4.3.4 Zircon .....	43
3.4.3.5 Cryolite .....	44
3.4.3.6 Columbite .....	44
3.4.3.7 Thorite .....	44
3.4.3.9 Cassiterite .....	45
3.4.4 Mineral Maps .....	45
3.4.5 Comparison of results with previous studies .....	49
3.4.6 Mineralogical textural analysis: Yttrifluorite distribution .....	49
3.4.7 Petrophysical analysis: Porosity .....	50
3.5 CONCLUSION .....	51
ACKNOWLEDGEMENTS .....	52
References .....	52



Chapter 4: ArcGIS™ Proximity and Cluster Analysis of Electron Probe Micromaps of Round Top Critical Mineral Deposit .....	52
4.1 ABSTRACT .....	57
4.2 INTRODUCTION .....	57
4.3 METHODS .....	59
4.3.1 Sample collection and preparation .....	59
4.3.2 Electron probe microanalysis .....	59
4.3.3 ArcGIS™ – Proximity Analysis .....	60
4.3.4 ArcGIS™ – Cluster Analysis .....	60
4.4 RESULTS AND DISCUSSION .....	62
4.4.1 Proximity analysis of yttrifluorite .....	62
4.4.2 Ripley’s K cluster analyses .....	64
4.4.2.1 Magnetite (Fe <sub>3</sub> O <sub>4</sub> , cubic) .....	65
4.4.2.2 Annite mica (KFe <sub>3</sub> <sup>2+</sup> AlSi <sub>3</sub> O <sub>10</sub> (OH) <sub>2</sub> , monoclinic) .....	66
4.4.2.3 Zircon (ZrSiO <sub>4</sub> , tetragonal) .....	67
4.4.2.4 Yttrifluorite (CaF <sub>2</sub> , isometric) .....	68
4.4.2.5 Cryolite (Na <sub>3</sub> AlF <sub>6</sub> , monoclinic) .....	69
4.4.2.6 Uraninite (UO <sub>2</sub> , isometric) .....	70
4.4.2.7 Thorite ((Th,U) SiO <sub>4</sub> , tetragonal) .....	71
4.4.2.8 Cassiterite (SnO <sub>2</sub> , tetragonal) .....	72
4.4.2.9 Columbite (Fe <sup>2+</sup> Nb <sub>2</sub> O <sub>6</sub> , orthorhombic) .....	73
4.4.2.10 Data summary .....	75
4.5 CONCLUSIONS .....	77
ACKNOWLEDGEMENTS .....	78
References .....	78
Curriculum Vita .....	83

## List of Tables

Table 3.1: Principal Component percentages of major, minor and accessory minerals with different filters. ....	37
Table 3.2: Principal Component List .....	38
Table 3.3: Comparison of Round Top Mountain rhyolite CIPW norm mineral compositions among authors. ....	48
Table 4.1: Number, size and proximity of yttrifluorite grains and neighboring minerals .....	63
Table 4.2: Summary of spatial cluster analysis of 9 minerals. ....	76

## List of Figures

Figure 2.1: Round Top Mountain rhyolite photo.....	4
Figure 2.2: Polished blocks and specimens of rhyolite variety. . . . .	8
Figure 2.3: Experimental setup of permeability slabs. ....	11
Figure 2.4: Drops of fountain ink in an open humidifying box. ....	12
Figure 2.5: Pre- and Post-Acid-Leach porosity. ....	13
Figure 2.6: Average Porosity of Pre- and Post-leaching. ....	15
Figure 2.7: Timed ink penetration of rhyolite slabs.....	17
Figure 2.8: Top and bottom of thick slabs with ink penetration. ....	17
Figure 3.1: Intensity map of EPMA samples.....	33
Figure 3.2 X-ray maps of elements K, Al, Si and Na with RGB of combined elements of sample RT 4. . . . .	40
Figure 3.3: X-ray maps of elements K, Al, Si and Na with RGB of combined elements of sample RT 7. ....	41
Figure 3.4: X-ray maps of elements K, Al, Si and Na with RGB of combined elements of sample RT 9. . . . .	42
Figure 3.5: Mineral maps of RT 2 and RT 12.....	46
Figure 3.6: Mineral maps of all 7 RT maps with major, minor and accessory minerals. ....	50
Figure 3.7: Mineral maps of sample RT 4 showing pore space.....	51
Figure 4.1: Mineral maps generated from EPMA using ArcGIS™ . . . . .	64
Figure 4.2: Cluster analysis results of magnetite.....	66
Figure 4.3: Cluster analysis results of mica. ....	67
Figure 4.4: Cluster analysis results of zircon.....	68
Figure 4.5: Cluster analysis results of yttrifluorite. ....	69

Figure 4.6: Cluster analysis results of cryolite. ....	70
Figure 4.7: Cluster analysis results of uraninite.....	71
Figure 4.8: Cluster analysis results of thorite. . ....	72
Figure 4.9: Cluster analysis results of cassiterite.....	73
Figure 4.10: Cluster analysis results of columbite. ....	74

## Chapter 1: Introduction

This project consists of three separate projects that all investigate Round Top Mountain, a rhyolite laccolith located in Sierra Blanca, west Texas in Hudspeth County (U.S.A). The three projects will explore and analyze the petrophysical, geostatistical and geo-spatial aspects of this unique deposit.

### Project 1:

This petrophysical study examines the porosity and micro-permeability of the Round Top rhyolite at a scale, roughly 5 to 10 mm or pebble sized, similar to anticipated heap leach crush sizes. Large voids and fluid paths, such as faults and joints in the massive rock (meter to km scale, boulder to outcrop size), are not germane to the proposed crushing and heap leach operations and thus were not examined. To simulate anticipated heap leach conditions, we therefore designed experiments based on penetration of water and water-based ink into our rock under Earth-surface temperature and atmospheric pressure. The experiments thus simulate anticipated heap leach conditions (aqueous solutions, ambient temperature and pressure).

### Project 2:

The purpose of this study is to create detailed mineralogical maps using multivariate statistical analysis and geospatial analysis through the use of ArcGIS™. These mineral maps can improve our understanding of the mineralization process that is unique to Round Top Mountain and inform approaches to potential extraction of that mineral wealth. This research is an extension of (Pingitore et al., 2017) where electron microprobe mapping was used to outline the microscopic distribution of heavy rare earth elements (HREEs) and better understand the mineralization and potential extraction processes.

### Project 3:

This research is an extension of previous works on the Round Top Mountain deposit. In this paper, mineral maps are further analyzed spatially through proximity and cluster analyses using tools in the ArcGIS™ software system. We also use the Ripley's K function to show how spatial clustering or dispersion of feature centroids change as neighborhood sizes change. The purpose of this study is to ascertain if specific minerals of potential economic value are clustered or disperse in the rhyolite. This information can aid in understanding the formation and possible extraction of the target critical elements.

## **Chapter 2: Porosity and Permeability of Round Top Mountain Rhyolite (Texas, USA) Favor Coarse Crush Size for Rare Earth Element Heap Leach**

### **2.1 ABSTRACT**

Water-saturation porosity and dye-penetration permeability measurements of Round Top Mountain rhyolite confirm that a ½-inch (13-mm) crush size would permit efficient acid heap leaching of yttrium and heavy rare earth elements (YHREEs) hosted in yttrifluorite, a YHREE-substituted variety of fluorite. Laboratory acid leaching has extracted up to 90% of the YHREEs. The bulk insoluble gangue mineralogy of the rhyolite, 90% to 95% quartz and feldspars, assures low acid consumption. Different crush sizes were weighed, soaked in water, and reweighed over time to determine water-penetration estimated porosity. Typical porosities were 1% to 2% for gray and 3% to 8% for pink varieties of Round Top rhyolite. The same samples were re-tested after soaking in dilute sulfuric to simulate heap leaching effects. Post-leach porosity favorably increased 15% in pink and 50% in gray varieties, due to internal mineral dissolution. Next, drops of water-based writing ink were placed on rhyolite slabs up to ~10 mm thick, and monitored over time for visual dye breakthrough to the lower side. Ink penetration through 0.5 to 2.5-mm-thick slabs was rapid, with breakthrough in minutes to a few hours. Pink rhyolite breakthrough was faster than gray. Thicker slabs, 4 to 10 mm, took hours to three days for breakthrough. Porosity and permeability of the Round Top rhyolite and acid solubility of the yttrifluorite host should permit liberation of YHREEs from the bulk rock by inexpensive heap leaching at a coarse and inexpensive nominal ½-inch (13-mm) crush size. The rate-limiting step in heap leach extraction would be diffusion of acid into, and back-diffusion of dissolution products out of, the crushed particles. The exceptional porosity and permeability that we document at Round Top suggest that

there may be other crystalline rock deposits that economically can be exploited by a coarse-crush bulk heap leach approach.

## 2.2 INTRODUCTION

Yttrium and the heavy rare earth elements (YHREEs) are vital components of the materials in the optical, electronic, and mechanical products that define 21<sup>st</sup> Century technologies [1]. Virtually, all YHREEs currently are sourced from the famed south China ionic clay deposits [2]. Taxation, regulatory policies, and environmental degradation are challenges to the steady supply of those elements. Expanded demand for select YHREEs might exceed supply in the future. Thus, there is a global search for alternative sources beyond China, driven by these factors, as well as by trade policies and economic considerations [3,4].

Round Top Mountain in Hudspeth County, west Texas, USA, is a surface-exposed peraluminous ( $\text{Al}_2\text{O}_3 > \text{Na}_2\text{O} + \text{K}_2\text{O} + \text{CaO}$ ) rhyolite laccolith, a mushroom-shaped igneous intrusion. The mountain is roughly 2 km in diameter and over 1200 m high, with a rhyolite mass estimated at some 1.5 billion tonnes (Figure 2.1) [5]. The rock is enriched in rare earth elements (REEs) in excess of 500 ppm, of which the economically desirable heavy REEs and yttrium (YHREEs) comprise approximately 72%. The rhyolite intrusion is Late Eocene in age, dated radiometrically at 36 Ma (million years) [6]. Although originally emplaced at shallow depth beneath the Earth's surface, subsequent erosion of the overlying strata has left this rock, more resistant to gradual weathering, as a prominent topographic feature. Thus, there is little or no overburden that would need to be removed to commence surface mining by blasting, moving, crushing, and stacking operations to prepare a heap leach pad.



**Figure 2.1.** Round Top Mountain yttrium and the heavy rare earth elements (YHREE) deposit, Hudspeth County, west Texas, USA. Virtually the entire mountain, extending a short distance into the subsurface, is mineralized. Note drill rig on peak for scale.

Round Top is enriched in a suite of incompatible elements, those that are due to their ionic radius and charge are not easily incorporated into common igneous rock-forming minerals. At Round Top, these include YHREEs, light REEs (LREEs), Sn, Be, Li, Cs, Rb, U, Th, Ga, Nb, and Ta. Although a number of REE-bearing minerals have been reported in the deposit, synchrotron-based X-ray absorption spectroscopy documented that yttrifluorite hosts essentially all of the YHREEs [7]. Yttrifluorite is a variety of the common mineral fluorite ( $\text{CaF}_2$ , isometric) in which the trivalent (3+) Y and HREEs substitute for ~5% to 30% of the bivalent  $\text{Ca}^{2+}$  cations, yielding the formula  $(\text{Ca}_{1-x}, \text{Y}, \text{HREE}_x)\text{F}_{2+x}$  [8]. No other yttrifluorite-hosted YHREE deposit has yet been described; the Round Top Mountain deposit mineralogy at present appears to be unique.

Mineralization is pervasive and homogeneous through the laccolith, with the exception of the rhyolite margins, where mineralizing fluids interacted with the enclosing country rock and concentrated or diluted various elements. YHREE mineralization occurred via pervasive



deposition from late stage (end of the magma cooling and solidification) fluorine-enriched fluid, in which the incompatible elements had concentrated [5,9,10].

The target YHREE-containing yttrifluorite occurs in the fine-grained matrix or groundmass of the rhyolite. Large crystals (up to perhaps 250  $\mu\text{m}$  in diameter) of feldspars and quartz formed during early slow cooling, and were encased in a fine-grained matrix that formed during rapid cooling when the magma was emplaced near the Earth's surface. Most of the yttrifluorite grains range from perhaps 10 to 1  $\mu\text{m}$  or less in diameter. The small size of the target yttrifluorite grains renders such conventional physical beneficiation techniques as froth flotation, gravity separation, magnetic separation, *etc.* uneconomical, chiefly, due to the extremely fine, and perhaps unachievable, particle size required to liberate the minuscule yttrifluorite crystals by sequential crushing, grinding, and milling. Nonetheless, yttrifluorite is soluble in dilute sulfuric acid and thus the deposit potentially could be exploited by heap leaching [11].

The Round Top deposit is situated on land owned by the State of Texas, currently leased by Texas Rare Earth Resources, Inc. (TRER, Sierra Blanca, TX, USA), a publically traded (US stock ticker TRER) mining exploration and development company. TRER has issued preliminary plans to extract the YHREEs, LREEs, and byproduct U, and possibly Be and Li, via low-cost heap leaching with dilute sulfuric acid [12,13].

In a heap leach operation, mineralized rock is blasted and crushed (and ground or milled to a fine particle size, if required), then placed in a large shallow pit previously lined with an impermeable barrier of clay or synthetic material. Crushed rock is stacked to a height of perhaps 10 m, and then irrigated from above with the solvent (in this case it would be dilute sulfuric acid). The leach solution percolates down through the pile, wetting surfaces of the particles. The solution reacts with both the external surface of the crushed particles, and with the interior of the

particles by infiltrating and saturating their contained micropore system. Leach solution is collected from the pit bottom, recharged with acid as needed, and recirculated or drawn off for removal of dissolved target and waste ions in an adjacent chemical processing plant [14].

Bench scale column test leaching of composite samples of Round Top rhyolite with dilute sulfuric acid yielded recoveries of up to 90% of the YHREEs at various crush sizes up to 0.5 inches (~13 mm) [13]. This observation suggests that the acid solvent solution is able to penetrate to the centers of such grains, as well as permeate most of the rock volume of the particle to achieve the nearly complete YHREE recoveries observed in the laboratory. These petrophysical qualities of the rhyolite are thus crucial to scaling the proposed leaching process from bench studies to pilot plant to industrial field operations.

This petrophysical study examines the porosity and micro-permeability of the Round Top rhyolite at a scale, roughly 5 to 10 mm or pebble sized, similar to anticipated heap leach crush sizes. Large voids and fluid paths, such as faults and joints in the massive rock (meter to km scale, boulder to outcrop size), are not germane to the proposed crushing and heap leach operations and thus were not examined. Note that use of the term micro-permeability reflects that the relevant fluid pathways in the crushed material occur chiefly at a micrometer ( $\mu\text{m}$ ) or smaller scale.

Porosity is defined as the volume of contained void space expressed as a fraction or percent of the total rock volume. This percentage varies dramatically with rock type and individual occurrence; some sedimentary rocks can exhibit 40% or more porosity, whereas igneous rocks, such as granite and rhyolite, typically have porosities in the low single digit range [15,16,17,18,19,20]. For most crystalline rocks (*i.e.*, igneous and metamorphic groups), porosity values are low due to formation of the rock at high temperatures and/or pressures. In

some igneous rock commercial deposits, the mineralizing hydrothermal solutions enhanced the original porosity and permeability.

Permeability is the ability of a rock to transmit fluids, typically water, gas, or oil. Unless extensively fractured, most crystalline rocks exhibit low permeabilities [19,21]. Thus, a slab of unbroken granite can be suitable for use as a kitchen counter top but does require a synthetic sealant to prevent minor penetration and staining.

In the petroleum industry, porosity and permeability are conventionally measured by the injection of mercury into a rock specimen under increasing pressure [22]. Although this technique is appropriate for the ambient pressures several or more kilometers deep in the Earth's subsurface, it is not relevant to the mild surface conditions in a heap leach. To simulate anticipated heap leach conditions, we therefore designed experiments based on penetration of water and water-based ink into our rock under Earth-surface temperature and atmospheric pressure. The experiments thus simulate anticipated heap leach conditions (aqueous solutions, ambient temperature and pressure).

## **2.3 MATERIALS AND METHODS**

### **2.3.1 Rhyolite Samples**

Two colors, pink and gray, dominate the rhyolite found at Round Top. Previous investigators have described 4 or 5 colors (pink, red, purple, gray, and tan, the latter of limited volume and occurring only in places at the borders of the deposit), with no formal distinctions; here, we use pink to include pink, red, and purple hues (Figure 2.2) [5,9,10]. Samples of the two colors are similar in elemental composition, with the pink hue resulting from the partial oxidation or rusting of magnetite ( $\text{Fe}_3\text{O}_4$ , isometric) grains [5,9,10,23]. In Round Top Mountain,

there are no sharp boundaries between these colors and intermediate shades are common. Because the oxidation may have been controlled by, and/or also altered, porosity and permeability, samples of both colors were tested and compared.



**Figure 2.2** Polished blocks and specimens of pink (including red and purple hues) and gray varieties of Round Top Mountain rhyolite. Note sub-mm size of the mineral grains. Scale = 16 cm.

Samples for analysis were taken from a large (several hundred kg), well-mixed composite of material recovered from numerous reverse circulation bore holes drilled at scattered sites across the deposit [13]. Crush sizes and size ranges were produced by conventional sieve separations or visual inspection and selection of particles on appropriately sized printed measurement grids.

### 2.3.2 Porosity Measurements

A total of 15 pink and 15 gray samples were chosen by hand from crushed material based on estimated size. Samples were divided into three particle size categories with 5 samples each: 5

mm × 5 mm (visual grid inspection), 5 to 10 mm (sieved), and 10 mm (visual grid). Sample sets, after weighing (between 5 and 11 g), were placed into 50-mL beakers containing a mixture of nine parts de-ionized water and one part tap water (to neutralize pH while limiting dissolved solids), covered, and allowed to soak.

Pre- and post-soak sample weights served to determine the mass of water that penetrated the samples during a 3-week period of immersion. The volume of pore space filled in this process was derived from the added water mass (with the calculation taking into account, of course, the respective densities of water and rhyolite). In order to accurately measure the gain in mass due to water infiltration of the interior pore space of each sample, but not due to water clinging on the exterior of the particle. It was imperative to dry the surface of the sample, while retaining the interior moisture. This was accomplished by quickly blowing air on the rock surface until it was visually dry. Dried samples exhibited a characteristic rough and dusty appearance, in contrast to the shiny clean surface when wet. Inasmuch as some interior moisture could be lost in this process, the weight gain and calculated porosity (more precisely stated, the estimated porosity) thus obtained can be considered a minimum. Nonetheless, repeated measures over time and examination and comparison of 5 multiple samples confirm the accuracy of the technique for determination of estimated porosity. Weights for all samples were recorded after 1, 2, 4, 8, 13, and 21 days.

Next, the Round Top samples were dried for 2 days. Then, samples were placed into beakers with 80 mL of 4.25% (v/v) H<sub>2</sub>SO<sub>4</sub> and left on a shaker table for 3 weeks. This simulates the initial, and most productive (the period during which most of the YHREEs are released), stage of the heap leach process, which would actually continue for up to 2 to 3 months. After 3 weeks, samples were rinsed 3 times with water and transferred into a clean beaker. Samples were again

left to soak for 24 h in the same type of water used for the porosity measurements to allow the diffusion of residual acid from the interior of the samples. This procedure was repeated twice. Samples were then removed from the water bath and left to air dry for 24 h before recording the new current dry weight. This weight was used to quantify the effects of the acid treatment in a second round of “post-acid-leach” porosity experiments. This procedure to simulate the heap leach would document anticipated increases in porosity due to the corrosive action of the acid. Note, of course, that under the field conditions of an industrial heap leach operation, increases in porosity would occur over considerably longer time scales than those modeled here at bench scale.

### **2.3.3 Permeability Measurements**

Both pink and gray samples of Round Top rhyolite were cut into parallel-sided slabs at staged thicknesses of up to 10 mm with the use of a low-speed circular saw with a diamond blade (Buehler Isomet™, Lake Bluff, IL, USA) and/or a coarse diamond grinding wheel. A single drop of consumer fountain pen ink (Parker Quink™, Newhaven, UK, washable blue) was placed on each slab and penetration breakthrough to the underside was tracked over time by observing the slab bottom in a mirror placed below the slabs (Figure 2.3). To prevent the ink drop from spreading laterally, and even bleeding down the sides of the sample slab, prior to placement of the drop, a small barrier ring was created on the slab surface with quick-drying clear fingernail polish. The ink was refreshed as needed, and water added when evaporation was seen to have concentrated and thickened the ink.

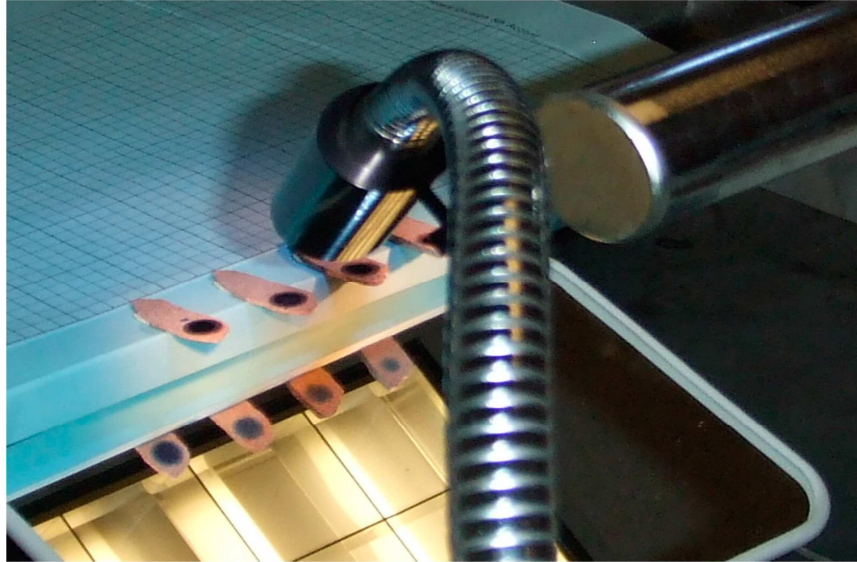


**Figure 2.3.** Experimental setup to permit simultaneous observation of ink applied to tops of slabs and image in mirror, angled below, of breakthrough ink on the undersides of slabs. Metal gooseneck piece in foreground is a high-intensity lamp.

Some thicker samples ( $>2.5$  mm), particularly of the gray variety, were found to require up to 2 to 3 days for penetration. Therefore, a shallow ( $<1$  mm deep) dimple was drilled into the upper surface to permit placement of a larger drop of ink. The samples were then placed into an airtight box containing water in open beakers that would maintain a high ambient humidity (Figure 2.4). This would slow evaporation and drying of the ink, which could clog the micropores and invalidate the experiment. Additional ink was added as it was lost to both evaporation and penetration of the rock. Penetration breakthrough and spread were documented photographically and time-recorded for the thin slabs.



**Figure 2.4.** Drops of fountain pen ink being applied to thick slabs of rhyolite in the open humidifying box. Beakers of water to maintain humidity visible at the bottom of box.

## 2.4 RESULTS

### 2.4.1 Pre-Acid-Leach Porosity

In the first set of trials (pre-acid leach), the pink rhyolites displayed overall higher porosities than the gray rhyolites, for all particle sizes (Figure 2.5a). Variation among the five individual particles measured in each experimental set was more pronounced for the pink rhyolites than for the grays. These two observations suggest that the magnetite (and possibly other minerals) oxidation reactions that created the pink color also created additional porosity and/or additional micro-permeability that permitted better penetration of the water in our experiments. Similarly, the magnetite oxidation might have been controlled by the prior distribution of permeability and porosity in the nearly solidified rhyolite.



## Porosity Pre-Acid Leach

## Porosity Post-Acid Leach

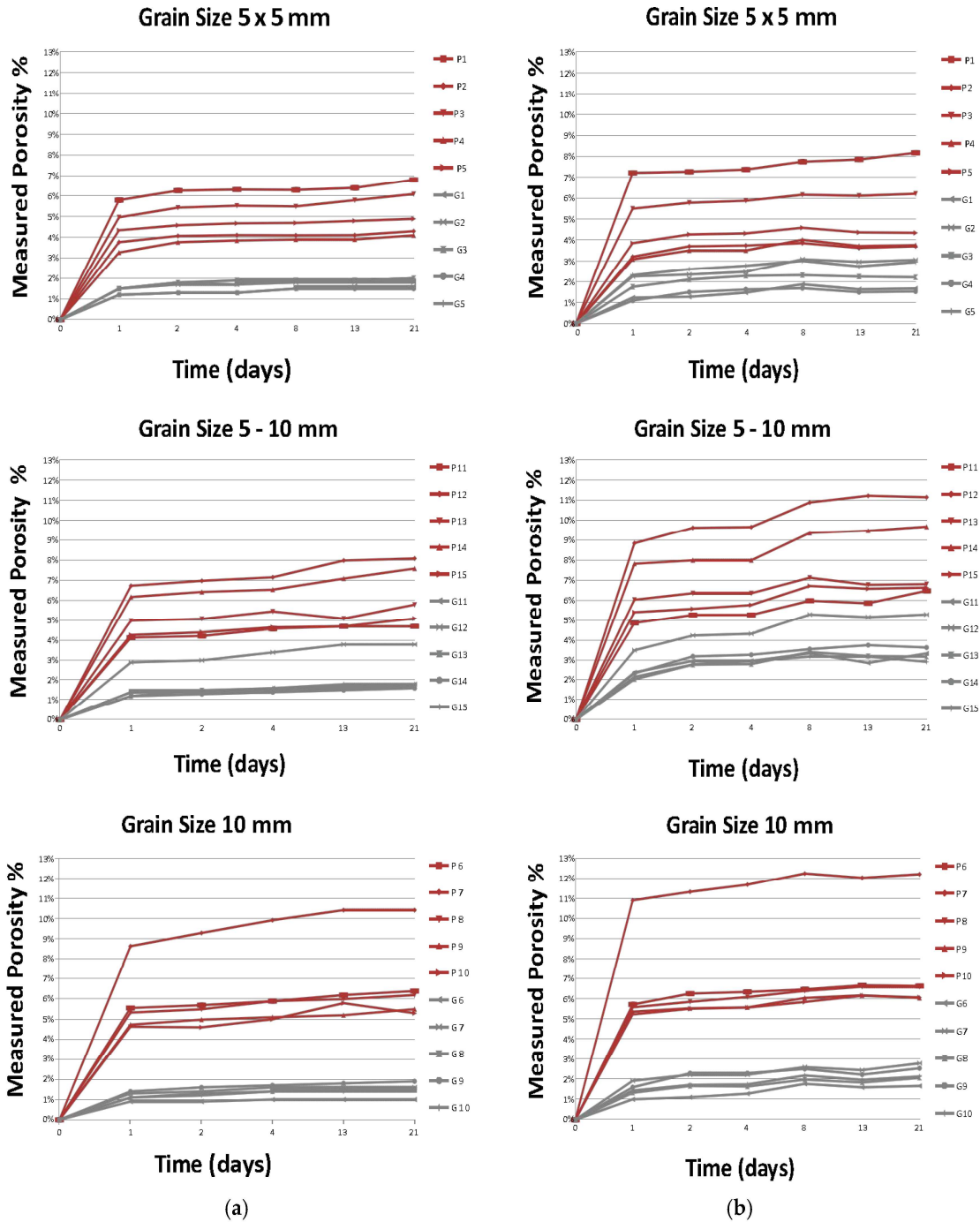


**Figure 2.5.** Estimated porosity measurements: (a) Pre-acid leach experiments; (b) Post-acid leach experiments. Red lines = pink samples; Gray lines = gray samples.

For each of the two individual colors, variation in porosity between particle sizes was relatively minor. We examined different sizes because of the possibility that potential errors in the surface drying process might be correlated with the different surface-area-to-volume ratio inherent in different particle sizes. A further consideration was the possibility that in larger particle sizes (imagine, at the extreme, a boulder) penetration of water to interior porosity might be extremely slow or even impossible, yielding a lower measured water-mass-gain porosity, or that smaller sizes might expose more internal pore space. The data indicate that none of these potential effects was a significant problem in the range of particle sizes tested.

The flattening of the curves of porosity *versus* time (Figure 2.5a) demonstrates that water saturation of the particles was approached in two to five days. The flattening is more pronounced for the pink rhyolites; some of the gray rhyolites appear to have absorbed minor additional quantities of water throughout the experimental period (slight positive slope to three weeks). The longer saturation time for the gray rhyolite is consistent with their lower porosity.

The largest water gain occurred during the first day, an effect confirmed in the permeability studies (Section 2.3.3.), where mm-scale dye penetration was observed at a time scale of minutes to a few days.

#### **2.4.2 Post-Acid-Leach Porosity**

In the second trial, porosities are seen to have increased overall after leaching with dilute sulfuric acid (Figure 2.5b). Further, the spread of the data, as seen in the vertical separation of the individual curves, is also greater. This is consistent with the addition of a new variable, the degree of interior corrosion by the acid leach, which potentially increases variation in the data. As in the first set of trials, the pink rhyolites exhibit higher overall porosities than the gray suite.

Interestingly, the approach to water saturation appears consistently to be approximately one week, about twice as long as observed in the pre-acid-leach experiments. This suggests the creation of additional micro-pores by mineral dissolution during the leaching period, which then require additional time to fill.

No porosity trends relative to grain size were evident; the 5 to 10 mm exhibited the highest overall porosities.

The pink rhyolites (all 15 samples used in the study) exhibited an average 15% increase in final porosity (21st day observation) from 6.1% pre-leach to 7.0% post-leach ([Figure 6](#)). The gray rhyolites (15 samples) averaged a 50% increase in final porosity, from 1.8% before leaching to 2.7% after leaching.

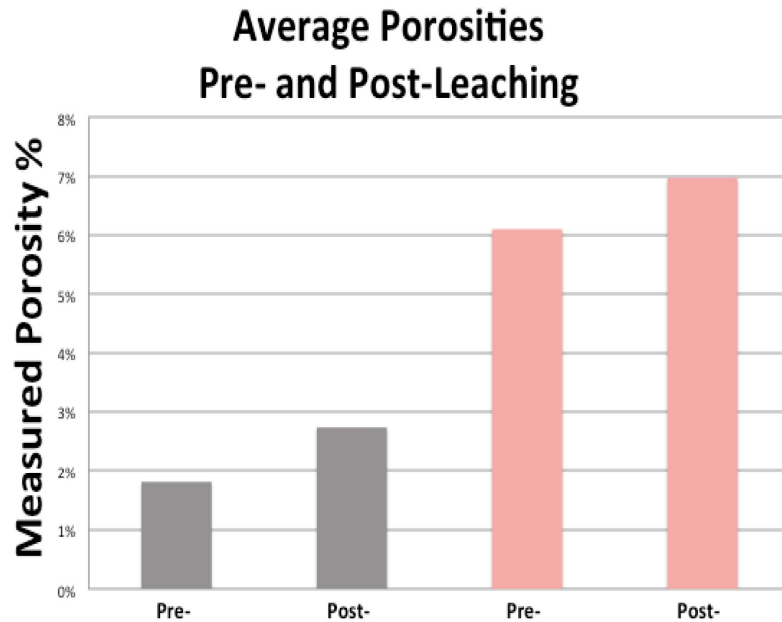


**Figure 2.6.** Average (15 samples per color) porosity pre- and post-leaching, showing an increase in porosity after sulfuric acid dissolution. Gray bars represent gray samples; red bars represent pink samples.

### 2.4.3 Permeability

Penetration of both the pink and gray rhyolites was rapid, and sequential in time with slab thickness ([Figure 7](#)). Within 30 min, breakthrough of the ink on all the pink and the gray rhyolite slabs with thickness to 2.5 mm had occurred. Greater thickness, 3 to 10 mm, took up to three days for breakthrough ([Figure 8](#)). This is consistent with the two to three days for the similarly sized porosity samples to approach water saturation. Of special significance is the observation that this initial penetration was focused, that is, the initial ink stain penetrations on the slab bottoms were circular and similar in size to those placed on the slab top. Lateral spreading of the ink at the lower surface of the slabs is only evident at some time well after initial breakthrough. This indicates that the fluid pathways from the top of the slabs to their bottoms were relatively direct. In light of this, it is evident that the micro-pore system in these rhyolites is pervasive and isotropic, with no evidence of preferred orientation of the fluid pathways. On the thick slabs, ink permeation is visible on the sides of many of the blocks, consistent with continued ink spreading during the longer time duration of these experiments.

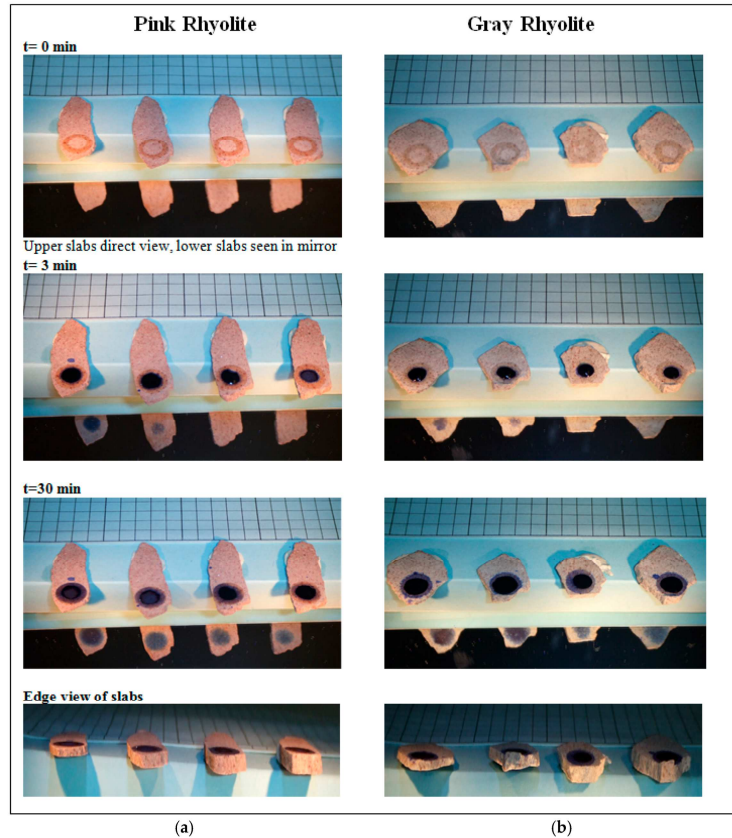


**Figure 2.7.** Timed ink penetration of rhyolite slabs to determine permeability. Boxes = 0.5 cm. **(a)** Pink rhyolite; **(b)** Gray rhyolite. Circles seen at  $t = 0$  are the ridges created by nail polish, which serve to contain and restrain the ink.

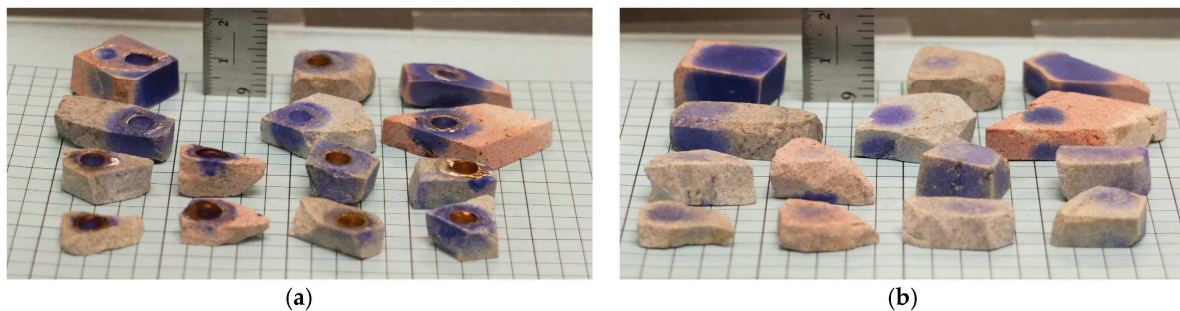


**Figure 2.8.** **(a)** Top surface of thick slabs with ink dimples; **(b)** Bottom surface of slabs showing ink breakthrough. Exposure times from six hours to three days. Top row of

samples, left to right: pink, gray pink; Second row: gray, gray pink; Third row: gray, pink, gray, gray; Bottom row: gray, pink, gray, gray.

One cautionary note: Once the ink penetrates to the bottom of the slab, it gradually spreads outwards from the transporting pore systems, migrating along the open lower surface. Thus, the ink-stained surface gives the appearance of a denser and more pervasive saturation than actually exists in the interior of the slab. Nonetheless, the stain indicates the general area reached by the micro-pore system in the rhyolite slab.

In general, the pink variety of rhyolites exhibited more favorable permeability than the gray rhyolite. This was particularly noticeable in tests of the thicker slabs (5 to 10 mm). Pink specimens typically required 6 to 24 h for breakthrough, whereas the grays required as long as three days for penetration.

## **2.5 DISCUSSION**

### **2.5.1 Significance of Round Top Rhyolite Porosity and Permeability**

The porosities measured on the Round Top rhyolite samples exceed those of such related rocks as granite, typically reported at 1% or less. Equally important, all samples proved visibly permeable, with rapid penetration and saturation of the particles. These properties contribute to the feasibility of heap leaching at a nominal crush size of ½ inch (13 mm). If the rock were not porous and permeable, it would be necessary to grind or mill to a much finer particle size for the acid to access the minuscule, scattered yttrifluorite target grains. Such mechanical processing would involve considerable expense, in capital equipment, operating costs, and complexity of

design. Further, finer particle sizes can lead to jamming of the fluid pathways of the percolating leach fluid, resulting in incomplete exposure of some particles and lower YHREE recoveries. The ink penetration permeability study demonstrated rapid particle penetration on samples up to 10 mm thick. This suggests that a crush particle 20 mm thick would be efficiently saturated by entry of the solution from all sides of the particle (10 mm radius). Thus, a ½ inch crush size is well within the range of successful testing in this study. It is important to realize that the loci of the YHREEs within the rhyolite apparently are closely associated with the primary porosity of the rock. The minerals hosting the YHREEs and associated incompatible elements were precipitated from a fluorine-rich vapor phase in the final stage of cooling of the magma. These last-stage minerals formed in the space that the vapor phase occupied, and in the pore space opened as the F-vapor corroded pre-existing feldspar crystals [10]. Consequent to this quirk of the rhyolite's genesis, a leach solution entering the micropores of a crush particle will contact most of the target yttrifluorite grains. Very few yttrifluorite grains can be expected to be “locked” in a matrix of acid-insoluble minerals, e.g., quartz and feldspar. This apparent geometric association of porosity and target yttrifluorite contributes significantly to the exceptional recoveries, up to 90%, encountered in both bottle roll and column test heap leach experiments at bench scale [13].

### **2.5.2 Heap Leach Efficiency: Pink vs. Gray Rhyolite Varieties**

The better performance characteristics of the pink rhyolite in porosity and permeability tests suggests that a heap leach with material solely of this color could achieve faster and perhaps more thorough YHREE recoveries. The distribution of these two varieties in Round Top Mountain would permit selective mining of either color variety. Overall, pink dominates the

upper portion of the mountain, gray the center, and pink the lower part. To extract primarily pink, one could mine the deposit from the top, or mine the lower slopes from the level of the surrounding desert. Given the huge size of the mountain, mining solely the pink could be carried out for many decades—tens and tens of years.

Alternatively, the rate of leaching in the heap pile could be slowed or moderated by the judicious mixing of pink and gray rhyolite. Such an approach could be an option if the leach is designed with separate piles, where the leach solution is shunted between different sections to regulate the concentration of ions delivered to the chemical recovery plant. Continuous delivery of a final leach solution of constant composition to the chemical plant is essential to its efficient operation.

### **2.5.3 Ionic Diffusion: Rate Limiting Step for Round Top Heap Leach**

The porosity and permeability experiments described herein are consistent with laboratory-scale sulfuric acid leaching experiments described elsewhere, and with unpublished data [13]. Initial dissolution of rare earths and other elements is rapid, with YHREE recoveries of ~33%, in the first 24 h, depending on acid strength and particle size. In bottle roll tests recoveries of 50% to 75% were achieved with 4-mm-diameter particles in one week, and 75% with 10-mm-diameter particles in two weeks. Nonetheless, REE recoveries were observed to increase, albeit with diminishing returns, with continued immersion in acid solution over the course of several to many weeks. Final recoveries of up to 90% for the target YHREEs were achieved in approximately 10 weeks in both bottle roll and column tests.

The time lapse between initial dissolution of YHREEs and near-complete dissolution indicates that transport of acid to the interiors of the particles, and back-transport of the YHREEs out of the particles, is an important rate-limiting step in the leaching process. On the one hand,



the permeability breakthrough data and the porosity saturation data indicate that aqueous solutions pass into the rhyolite rapidly, typically taking less than three days to penetrate to the center of a 13-mm-diameter particle (the anticipated crush size for the heap leach). On the other hand, it is obvious that efficient two-way advective transport of the leach solution into and out of the grains is not possible due to the micron to sub-micron dimension of the cracks through which such transport apparently occurs. There is no drive mechanism to push the leach solution in and then back out of these micro-cracks. At crack widths of this scale, capillary force dominates gravity force, and flow through or in and out of the particles does not proceed at economically favorable time scales. Diffusion of acid into the pores and back-diffusion of YHREE and other dissolved species out of the pores will be the most important drive mechanism for YHREE extraction in the heap leach. It is anticipated that diffusion thus will be the rate limiting step in the process. The dynamics of two-way diffusion between aqueous solutions in cracks in rock particle interiors and an external buffering solution has been described in detail in the literature [\[24\]](#).

#### **2.5.4 Unconventional Opportunity to Heap Leach Coarse-Crushed Crystalline Rock**

heap leaching of relatively unaltered crystalline rock is not a conventional mineral resource extraction technique. Typically, only carefully selected high-grade areas of hard rock mineral deposits are ever mined, crushed and heap leached. Bulk crystalline deposits occasionally can be crushed to a fine particle size and heap leached, e.g., the 5-mm crush size at the Etango uranium project [\[25\]](#). The exceptional porosity and permeability for a crystalline rock that we documented at Round Top present the opportunity to heap leach the bulk deposit at a

coarse crush size. This finding suggests that there may be other crystalline rock deposits that economically can be exploited for rare earths and other elements by a similar strategy.

## 2.6 CONCLUSIONS

- (1) Water-saturation porosity of Round Top rhyolite ranged from 1%–10%, with the pink variety consistently higher than the gray variety.
- (2) Water penetration and saturation was rapid, with most occurring within one day, and nearly complete in two to three days.
- (3) Porosity increased 15% (pinks) to 50% (grays) after a three-week dilute sulfuric acid leach.
- (4) Ink-penetration permeability was rapid (minutes to hours) for slabs up to 2.5 mm. Thicker slabs, to 10 mm, took as much as several days. Pink rhyolite was consistently more permeable than gray rhyolite.
- (5) The rate-limiting step for YHREE recovery in the anticipated heap leach is expected to be diffusion of fresh acid from the dripping heap leach solution into the solution-saturated micropores, and back-diffusion of dissolved elements out of the pores.

In light of these findings, the ½-inch (13 mm) crush size proposed by Texas Rare Earth Resources, Inc. for their heap leach design appears sound, and even conservative. Further, the

conclusions suggest that bulk coarse-crush heap leaching of other crystalline rock deposits with favorable porosity and permeability may be economical.

The ultimate success of the proposed Round Top Mountain YHREE heap leach will depend not just on the favorable estimated porosity and permeability documented here. Such other factors as wetting of the particles, clay formation or release, presence of fines, chemical reactivity leading to precipitation of secondary compounds, *etc.* all will play a role [26,27,28,29]. Typical heap leach recoveries for such ore deposits as copper porphyries are in the 60% range, significantly less than the 90% achieved in laboratory scale column tests of Round Top rhyolite. This suggests that tall column field scale tests are a logical next step in evaluating and “de-risking” heap leaching of the Round Top deposit.

## ACKNOWLEDGEMENTS

The authors thank Texas Rare Earth Resources, Inc. for access to samples and technical data. This project was supported by research contracts 26-8211-12 and 26-8211-16 between Texas Rare Earth Resources, Inc. and the University of Texas at El Paso. Funds for covering the costs to publish in open access were obtained from this source.

## References

1. Chakmouradian, A.R.; Wall, F. Rare earth elements: Minerals, mines, magnets (and more). *Elements* **2012**, *8*, 333–340. [[Google Scholar](#)] [[CrossRef](#)]
2. Peishan, Z.; Zhuming, Y.; Kejie, T.; Xueming, Y. *Mineralogy and Geology of Rare Earths in China*; Science Press: Beijing, China, 1995; p. 209. [[Google Scholar](#)]

3. Mariano, A.N. Economic geology of rare earth elements. In *Geochemistry and Mineralogy of Rare Earth Elements. Reviews in Mineralogy 21*; Lipin, B.R., McKay, G.A., Eds.; Mineralogical Society of America: Washington, DC, USA, 1989; pp. 309–337. [[Google Scholar](#)]
4. Mariano, A.N.; Mariano, A., Jr. Rare earth mining and exploration in North America. *Elements* **2012**, *8*, 369–376. [[Google Scholar](#)] [[CrossRef](#)]
5. Price, J.G.; Rubin, J.N.; Henry, C.D.; Pinkston, T.L.; Tweedy, S.W.; Koppelaar, D.W. Rare-metal enriched peraluminous rhyolites in a continental arc, Sierra Blanca Area, Trans-Pecos Texas; chemical modification by vapor-phase crystallization. In *Ore Bearing Granite Systems; Petrogenesis and Mineralizing Processes (Special Paper (Geological Society of America))*; Stein, H.J., Hannah, J.L., Eds.; Geological Society of America: Boulder, CO, USA, 1990; pp. 103–120. [[Google Scholar](#)]
6. Henry, C.D.; McDowell, F.W.; Price, J.G.; Smyth, R.C. *Compilation of Potassium-Argon Ages of Tertiary Igneous Rocks, Trans-Pecos, Texas*; University of Texas, Bureau of Economic Geology: Austin, TX, USA, 1986; pp. 1–34. [[Google Scholar](#)]
7. Pingitore, N., Jr.; Clague, J.; Gorski, D. Round Top Mountain (Texas, USA), a massive, unique Y-bearing-fluorite-hosted heavy rare earth element (HREE) deposit. *J. Rare Earths* **2012**, *32*, 90–96. [[Google Scholar](#)] [[CrossRef](#)]
8. Yttrifluorite, Mindat.org. Available online: <http://www.mindat.org/gallery.php?min=4371> (accessed on 27 December 2015).

9. Rubin, J.N.; Price, J.G.; Henry, C.D.; Koppenaar, D.W. Cryolite-bearing and rare metal-enriched rhyolite, Sierra Blanca Peaks, Hudspeth County, Texas. *Am. Mineral.* **1987**, *72*, 1122–1130. [[Google Scholar](#)]
10. O'Neill, L.C. REE-Be-U-F Mineralization of the Round Top Laccolith, Sierra Blanca Peaks, Trans-Pecos, Texas. Master's Thesis, University of Texas, Austin, TX, USA, 2014. [[Google Scholar](#)]
11. Crawford, J. Solubility Data on 646 Common and Not so Common Minerals, 2009. Available online: <http://www.mindat.org/article.php/553/Solubility+Data+on+646+Common+and+Not+So+Common+Minerals> (accessed on 27 December 2015).
12. Texas Rare Earth Resources. Available online: <http://www.trer.com> (accessed on 27 December 2015).
13. Gustavson Associates. NI 43–101 Preliminary Economic Assessment, Round Top Project, Sierra Blanca, Texas. 2012. Available online: [http://trer.com/wp-content/uploads/2012/06/TRER\\_NI%2043-101%20PEA\\_KLG\\_037.pdf](http://trer.com/wp-content/uploads/2012/06/TRER_NI%2043-101%20PEA_KLG_037.pdf) (accessed on 27 December 2015).
14. Dhawan, J.; Safarzadeh, M.S.; Miller, J.D.; Rajamani, R.K.; Moats, M.S. Insights into heap leach technology. In Proceedings of the 2012 SME Annual Meeting and Exhibit 2012, Washington, DC, USA, 19–22 February 2012; pp. 560–567.
15. Akinyemi, O.A.; Alabi, A.A.; Ojo, A.I.; Adewusi, O.E. Characterization of density and porosity of rocks samples from Ogun State of Nigeria. *Earth Sci. Res.* **2012**, *1*, 137–146. [[Google Scholar](#)] [[CrossRef](#)]

16. Bongiolo, E.M.; Bongiolo, D.E.; Sardini, P.; Mexias, A.S.; Siitari-Kauppi, M.; Gomes, M.E.B.; Formoso, M.L. Quantification of porosity evolution from unaltered to propylitic-altered granites: The <sup>14</sup>C-PMMA method applied on the hydrothermal system of Lavras do Sul, Brazil. *Ann. Acad. Bras. Ciênc.* **2007**, *79*, 503–517. [[Google Scholar](#)] [[CrossRef](#)]
17. Takarli, M.; Prince-Agbodjan, W. Temperature effects on physical properties and mechanical behavior of granite: Experimental investigation of material damage. *J. ASTM Int.* **2008**, *5*, 1–13. [[Google Scholar](#)]
18. Petford, N. Controls on primary porosity and permeability development in igneous rocks. In *Hydrocarbons in Crystalline Rocks*; Petford, N., McCaffrey, K.J.W., Eds.; Geological Society Publishing House: Bath, UK, 2003; pp. 93–107. [[Google Scholar](#)]
19. Brace, W.F. Permeability of crystalline rocks: New *in situ* measurements. *J. Geophys. Res.* **1984**, *89*, 4327–4330. [[Google Scholar](#)] [[CrossRef](#)]
20. Ilankoon, I.; Neethling, S. The effect of particle porosity on liquid holdup in heap leaching. *Miner. Eng.* **2013**, *45*, 73–80. [[Google Scholar](#)] [[CrossRef](#)]
21. Sausse, J.; Genter, A. Types of permeable fractures in granite. In *Petrophysical Properties of Crystalline Rocks*; Harvey, P.K., Brewer, T.S., Pezard, P.A., Petrov, V.A., Eds.; Geological Society Publishing House: Bath, UK, 2005; pp. 1–14. [[Google Scholar](#)]
22. Monicard, R.P. *Properties of Reservoir Rocks: Core Analysis*; Éditions Technip: Paris, France, 1980; pp. 1–168. [[Google Scholar](#)]
23. Pingitore, N.; Clague, J.; Gorski, D. Uniform distribution of yttrium and heavy rare earth elements in Round Top Mountain rhyolite deposit, Sierra Blanca Texas, USA:

- Data, significance, and origin. In Proceedings of the American Geophysical Union, Fall Meeting, San Francisco, CA, USA, 15–19 December 2014.
24. Pingitore, N. The role of diffusion during carbonate diagenesis. *J. Sed. Petrol.* **1982**, *52*, 27–29. [[Google Scholar](#)]
25. Bannerman Resources. Available online: <http://32uo991mljzg3wrz8dkq0et1.wpengine.netdna-cdn.com/wp-content/uploads/2015/07/Etango-Heap-Leach-Demonstration-Program-Phase-1-Report.pdf> (accessed on 12 December 2015).
26. Bartlett, R. *Solution Mining: Leaching and Fluid Recovery of Materials*, 2nd ed.; Gordon and Breach: Amsterdam, The Netherlands, 1998; p. 470. [[Google Scholar](#)]
27. De Andrade Lima, L. Liquid axial dispersion and holdup in column leaching. *Miner. Eng.* **2006**, *19*, 37–47. [[Google Scholar](#)] [[CrossRef](#)]
28. Petersen, J.; Dixon, D. Modelling zinc heap bioleaching. *Hydrometallurgy* **2007**, *85*, 127–143. [[Google Scholar](#)] [[CrossRef](#)]
29. Ilankoon, I.; Neethling, S. Hysteresis in unsaturated flow in packed beds and heaps. *Miner. Eng.* **2012**, *35*, 1–8. [[Google Scholar](#)] [[CrossRef](#)]

## **Chapter 3: ArcGIS™ and Principal Component Analysis of Probe Data to Micro-map Minerals in Round Top Rare Earth Deposit**

### **3.1 ABSTRACT**

Rare earth elements (REEs), especially heavy rare earth elements (HREEs), are in demand for their current and emerging applications in advanced technologies. Here we perform computer-driven micro-mapping at the millimeter scale of the minerals that comprise Round Top Mountain, in west Texas, U.S.A. This large rhyolite deposit is enriched in HREEs and such other critical elements as Li, Be, and U. Electron probe microanalysis of 2 x 2 mm areas of thin sections of the rhyolite produced individual maps of 16 elements. These were superposed to generate a 16- element composition at each pixel. X-ray Map Analyzer (XRMA), an ArcGIS™ tool, performed principal components analysis (PCA) on the elements, taken as variables, in those pixels, taken as samples. The derived PCs proved to be easily identified mineral compositions. The pixels were then relabeled as the appropriate minerals, thereby converting each of the 16 element maps into a single mineral map. The overall mineral composition of the 7 studied samples compared favorably with bulk analyses of the Round Top deposit available in the literature. Likewise the range of porosity in the maps was consistent with that of previous direct measurements by water saturation. Some of the HREE-target yttrifluorite grains were seen to cluster with other valuable incompatible elements, e.g., columbite, uranite, and cassiterite; all were emplaced by a late-stage fluorine carrier fluid. This new statistical and GIS-based technique provides a robust and unbiased approach to electron microprobe mapping.



## 3.2 INTRODUCTION

Round Top Mountain, a Tertiary rhyolite laccolith in Hudspeth County, west Texas, USA is a potentially economically valuable deposit of heavy rare earth elements (HREEs) and other critical elements (Rubin et al., 1987; Price et al., 1990; Pingitore et al., 2012; O'Neill et al., 2014; Negrón et al., 2016; O'Neill et al., 2017; Pingitore et al., 2017; Jowitt et al., 2017; Elliott et al., 2017; Pingitore et al., 2018a; Pingitore et al., 2018b). The rare earth element (REE) concentrations are over 500 ppm, of which approximately 72% are the desirable yttrium heavy rare earths (YHREEs), making it a globally significant deposit (Pingitore et al., 2012; Jowitt et al., 2017). Mineralization is homogenous throughout the laccolith with the exception of the rhyolite margins and synchrotron-based X-ray absorption spectroscopy shows that yttrifluorite hosts almost all of the YHREEs (Pingitore et al., 2012).

The purpose of this study is to create detailed mineralogical maps from thin sections of Round Top Mountain samples using a new approach that combines multivariate statistical analysis and geospatial analysis through the use of ArcGIS™ (Ortolano et al., 2014). These mineral maps will improve our understanding of the mineralization process at Round Top Mountain and inform approaches to potential extraction of that mineral wealth. This research is an extension of (Pingitore et al., 2017) where electron microprobe mapping was used to outline the microscopic distribution of heavy rare earth elements (HREEs) and better understand the mineralization and potential extraction processes.

### 3.2.1 Background

Round Top Mountain is a Tertiary rhyolite laccolith in Hudspeth County, Texas, U.S.A. It is a mushroom-shaped, peraluminous igneous intrusion that is roughly 2000 m in diameter and

over 375 m high, with a mass estimated at 1.6 billion tons. The rhyolite is composed mainly of Si, O, K, Al, and Na. Round Top Mountain underwent chemical alteration by a late-stage fluorine vapor phase that enriched it in HREEs and other incompatible elements (Price et al., 1990; Gustavson Associates, 2013; O'Neill et al., 2017). In the search for and delineation of mineral deposits from Round Top Mountain previous studies (Pingitore et al., 2012; Pingitore et al., 2017; Pingitore et al., 2018a; Pingitore et al., 2018b) have included standard methods such as the collection of rock samples and preparation of thin sections for analysis with optical petrography and scanning electron microscopes. Electron probe microanalysis (EPMA) uses a particle-beam technique to determine the elemental composition of individual grains or portions of grains in thin sections (Khashgerel et al., 2008). These analyses confirm the presence of major, minor, and trace elements of potential value within those mineral grains.

The previous studies defined the mineral deposits and confirmed the potential resource but they did not provide definite information on how to extract the desired minerals efficiently and economically. For that reason, we conducted further analyses, including more experimental techniques, to try to establish a basis for recovering the HREEs at Round Top Mountain economically.

### 3.3 SAMPLE SOURCE AND PREPARATION

For this study we used EPMA to estimate the concentrations of various elements and rastering to produce two-dimensional intensity maps of those elements for each thin sections. Spatial correlations (overlays) and other statistical manipulations between the intensity maps of the individual elements were used to convert the intensity maps to estimated mineral maps that show the size, shape, spatial distribution, grain “locking”, and other attributes of the target economic mineral(s) to aid in the determination of the feasibility and potential mechanism for their profitable extraction.

Multivariate statistical techniques, specifically principal component analysis (PCA), were applied to the EPMA intensity maps to define how elements are spatially correlated and how these clusters represent specific gangue and target minerals. PCA has been used in previous geological studies, for example, to assess the economic potential of a deposit based on its size (Rambert, 2005), to differentiate between enrichment and pollution of toxic elements in soils (Borůvka et al., 2005), and to locate hydrothermal alteration zones associated with metallic deposits (Crósta et al., 2003).

We also use the ArcGIS™ software to analyze the spatial distribution of the chemical elements in the thin sections expanding on the technique introduced by Ortolano and others (2014). ArcGIS™ is widely used in mining applications for geo-spatial analyses, such as mapping ore bodies and mineral (Sprague et al., 2006) and monitoring potential hazards related to mining production (Gasser et al., 2015). However, Ortolano and others (2014) first applied the software to X-ray maps from a scanning electron microscope (SEM) equipped with an energy dispersive X-ray detector system (EDS), along with multivariate statistics, to create multispectral images that illustrated compositional and microtextural relationships in rocks (Ortolano et al.,

2014). We utilized their methods to expand the study at Round Top Mountain to produce detailed information on the distribution and associations of minerals at that site.

### **3.3.1 Sample collection**

Texas Mineral Resources Corporation, a publically traded (stock ticker TMRC) junior mining explorer interested in developing Round Top, contracted an extensive program of reverse circulation drilling to delineate mineralization in the rhyolite. As part of their testing programs, they created a composite sample of several hundred kilograms of material taken from >100 drill holes. We chose random pieces from that composite, constrained only by a size, about 2 or 3 cm, large enough to fabricate a petrographic section.

### **3.3.2 Thin section preparation**

Samples were cut to provide a mounting surface, then ground flat and glued to a petrographic glass slide. Samples were sliced close to the glass and ground to the standard thickness of 30  $\mu\text{m}$ . The thin sections were polished to a mirror finish, and finished with a 0.05- $\mu\text{m}$  gamma aluminum oxide powder. Polished thin sections underwent an ultrasonic cleaning bath, an ethanol rinse, and carbon coating prior to analysis. Thin section preparation procedure followed Pingitore et al. (2017).

### **3.3.3 Electron probe microanalysis**

We mapped the elemental composition of our samples on a Cameca SX-50 (upgraded to SX-100 performance) electron probe microanalyser (EPMA) with 4 wavelength dispersive spectrometers (WDS). Instrument settings were 20 KeV accelerating electron beam voltage and 200 or 250 nA current, as imprinted on the images that follow. For each sample a randomly

selected 2 x 2 mm area was raster-scanned repeatedly in WDS mode to yield 516 x 516 pixel maps of Fe, K, Al, Si, Nb, Ca, Na, F, Sn, Th, Zr, Rb, Dy, U, Yb, and Y, plus a back scattered electron (BSE) map. The quality of an X-ray map depends on, among other factors, the particular element, its concentration, dwell time of the beam on each pixel, diffracting crystal detector, and the beam current. Similarly, brightness contrasts in the map depend on the differences in concentration of the element between or within the different phases of any sample. Fig. 3.1 shows an example of two of these intensity maps obtained for potassium (K) and iron (Fe).

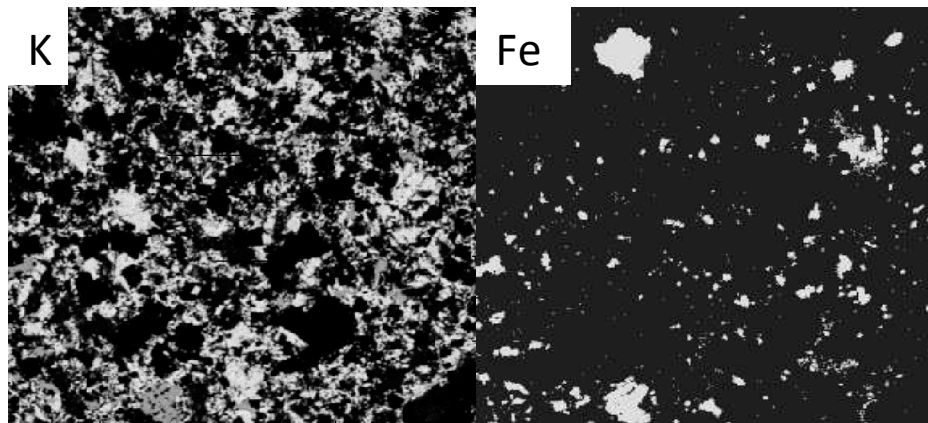


**Figure 3.1** Intensity maps obtained by EPMA of sample RT 10 thin section for elements potassium (left) and iron (right). Brighter areas indicate higher concentrations of the element. Field of View (FOV) 2 x 2 mm.

The BSE image displays pixels containing higher atomic number elements ( $Z$ ) as “bright” areas and those with lower  $Z$  elements as darker. Thus average  $Z$  within a pixel determines its relative brightness. The BSE images are helpful for quickly distinguishing different phases. X-ray element maps show the spatial distribution of elements in a sample. Maps of different

elements over the same area can help to determine the phases that are present and give a picture of any internal chemical zonation within a mineral.

### **3.3.4 X-ray Map Analyzer**

The X-ray Map Analyzer (XRMA) tool developed in Python™ and integrated with ArcGIS™ (Ortolano et al., 2014) allows the user to conduct principal component analysis (PCA), with the choice of no filter, a low pass filter, or a focal median filter. Applying different filters to the original X-ray maps can reduce or eliminate background noise, refining the principal components. A low pass, averaging filter traverses a 3-by-3 pixel filter over the input raster and smooths the data by taking the mean for each 3 x 3 area. A focal median neighborhood filter takes the shape of a neighborhood (i.e., circle or rectangle) and processes the map cells accordingly. Similar results were obtained using the low pass filter and the rectangular focal median filter. For comparison, we examined the element maps using a low pass filter and a circle focal median filter with a radius of 2 cells. The greatest asset to using XRMA is that it eliminates decision-making by the user and highlights textural features that are not obvious in optical microscopy or BSE images of thin sections (Ortolano, 2014).

### **3.3.5 Principal Component Analysis**

PCA defines a multidimensional coordinate system, where each axis is known as a principal component (PC). PCs can be considered as new super variables that replace sets of variables that are correlated, or in our case, sets of elements that are spatially correlated. In our application, we can consider a PC as likely representing a mineral present in the sample. In general, the largest portion of the information in a data set is found within the first three to five PCs. In our thin sections the first 3 PCs corresponded to the three major minerals found at Round

Top. The following few PCs described minor and accessory minerals. This paper will discuss the first 6 PCs due to their importance and relevance to this economic deposit.

### **3.3.6 ArcGIS™**

The ArcGIS™ raster calculator tool was used to take multiple individual element X-ray maps such as K, Al, and Si and integrate them to create separate mineral maps, e.g., K-spar, by displaying the pixels in which only those three elements occur together. These individual mineral maps were further refined using the reclassify tool to lower background noise, which narrows the data by labeling pixels with the highest intensity of the mineral with (1) and where it is not (0). Refined maps thus are generated delineating only where the mineral is present, and leaving the map open where the mineral is not present. This allows the analyst to connect the different layers of individual maps and see potential overlapping of minerals or pore space.

### **3.3.7 Integrating EPMA, XRMA-PCA, and ArcGIS™**

Our overall initial data processing comprised this flow: (1) generate X-ray maps from the EPMA; (2) input the X-ray map into XRMA to determine PCs using no filter, low pass filter, and circle focal median filter; (3) compare the spatial abundance of each PC as calculated in ArcGIS™ to percent mineral compositions obtained from prior research articles.

## **3.4 RESULTS AND DISCUSSION**

### **3.4.1 Principal Component Analyses**

We compared our results with previous analyses by Rubin et al. (1987), Gustavson Associates (2013), Shannon (1986), O'Neill (2014), and O'Neill et al. (2017) to test the validity and optimum methodology of the combined PCA and Arc GIS™ methods. The PCA images

generated using the low pass filter yielded the best results overall. Results with no filter appeared noisy and those with the circle focal median filter removed too much of the data. Sample RT 9, without a filter, did not produce coherent results and thus is not shown in Table 1. Also, zirconium (Zr) was not input into XRMA for RT 10 since the EPMA x-ray map was analyzed under different conditions, thus zircon is not present. The computer-generated mineral compositions based on the low pass filtered PCA data fall within range of mineral percentages found in prior research (Table 1) indicating our approach works well. The advantage of the computer-generated approach is that we were able to image smaller minerals and generate a more detailed map of the element locations that previous studies could provide. This is important in analyzing methods for mineral extraction at Round Top Mountain because the principle mineral, yttrifluorite, is typically less than 20  $\mu\text{m}$  in length.



**Table 3.1:** Principal component percentages of major, minor, and accessory minerals with different filters. Literature values are given at top for comparison to computer-generated results, below. NF = No filter; LPF = low pass filter; FMF = focal median filter.

Mineral %	Potassium Feldspar	Quartz	Sodium Feldspar	Annite Mica	Magnetite	Zircon	Yttrifluorite	Cryolite	Thorite	Uraninite	Cassiterite	Columbite
<b>EPMA sample</b>												
RT 2 - NF	41	17	22	7.8	2.0	0.3	0	0	0.4	0.1	0	0.8
RT 2 - LPF	44	20	23	4.9	2.1	0.8	0	1.3	0.1	0.1	0	0.3
RT 2 - FMF	45	25	21	3.2	3.0	1.5	0.2	0.8	0.1	0.04	0.1	0.2
RT 4 - NF	44	18	15	7.9	2.2	0.4	0	0	0.4	0.1	0.5	0.9
RT 4 - LPF	48	21	15	5.2	2.2	0.6	0.2	0.8	0	0.1	0.02	0.3
RT 4 - FMF	48	22	18	4.2	2.8	0.8	0.3	0.6	0.1	0.03	0.2	0.2
RT 7 - NF	50	18	13	3.3	1.6	0.2	0	0	0	0.12	0.7	0.8
RT 7 - LPF	54	21	14	4.5	1.2	0.4	0.1	1.1	0.1	0.01	0.1	0.2
RT 7 - FMF	55	22	15	2.5	1.4	0.5	0	0.5	0.1	0.02	0	0.2
RT 8 - NF	46	16	11	3.4	1.9	0.4	0.3	1.9	0	0.1	0.9	1.1
RT 8 - LPF	50	19	7.8	2.2	1.7	0.2	0.3	1.6	0	0.06	0.02	0.4
RT 8 - FMF	53	20	8.3	3.1	1.6	0.1	0.3	0.1	0.1	0.04	0.2	0.1
RT 9 - NF	0	0	0	0	0	0	0	0	0	0	0	0
RT 9 - LPF	52	20	8.6	5.1	1.3	0.2	0.5	0.9	0.1	0.1	0.05	0.2
RT 9 - FMF	56	21	10	3.7	1.7	0.8	0.4	1.7	0.1	0.1	0.04	0.2
RT 10 - NF	48	24	11	6.7	4.8	0	0.2	0.6	0.4	0.1	0.1	0.9
RT 10 - LPF	51	27	12	2.7	4.7	0	1.7	1.7	0.1	0.03	0.04	0.3
RT 10 - FMF	52	28	12	2.4	4	0	0.2	0.1	0.1	0.02	0	0.2
RT 12 - NF	47	20	10	1.5	1.0	0.4	0	1.1	0	0.1	0	0.8
RT 12 - LPF	51	23	11	5.1	1.0	0	0.4	0.4	0.1	0.01	0.02	0.2
RT 12 - FMF	52	23	13	3.5	1.2	0.6	0.2	0.9	0.1	0.02	0.01	0.2

**Table 3.2.** Principal component list

	RT 2	RT 4	RT 7	RT 8	RT 9	RT 10	RT 12
PC 1	K-spar	K-spar	K-spar	K-spar	K-spar	K-spar	K-spar
PC 2	albite	quartz	quartz	quartz	quartz	quartz	quartz
PC 3	quartz	albite	albite	albite	albite	albite	albite
PC 4	mica	mica	mica		mica	magnetite	mica
PC 5				mica		mica	
PC 6	magnetite		magnetite		magnetite	YF	
PC 7	cryolite	magnetite	cryolite	magnetite	zircon	cryolite	magnetite
PC 8		cryolite		YF	cryolite		cryolite
PC 9	zircon	zircon		cryolite	YF		YF
PC 10	columbite	columbite	zircon	columbite		columbite	
PC 11		YF	columbite	zircon	columbite		columbite
PC 12	YF						
PC 13			YF	thorite	thorite		thorite
PC 14	thorite	thorite	thorite	uraninite	uraninite	thorite	uraninite
PC 15	uraninite	uraninite	cassiterite			cassiterite	
PC 16	cassiterite	cassiterite	uraninite	cassiterite	cassiterite	uraninite	cassiterite

### 3.4.2 Principal Components: Major Minerals

In all 7 thin sections the highest weighted variables comprising the first 3 PCs were K, Al, Si, and Na. These four elements are known from bulk elemental analyses (Pingitore et al., 2017) to make up 80-90% of Round Top rhyolite. The three minerals corresponding to the first 3 principal components are the major minerals of the Round Top rhyolite: orthoclase feldspar (K-spar,  $\text{KAlSi}_3\text{O}_8$ , monoclinic), plagioclase feldspar (albite,  $\text{NaAlSi}_3\text{O}_8$ , triclinic) and quartz ( $\text{SiO}_2$ , trigonal). Figs. 3.2, 3.3, and 3.4 are X-ray maps for K, Al, Si, and Na, along with larger red-green-blue (RGB) maps of the first 3 principal components, for samples RT 4, RT 7 and RT 9. The X-ray maps, represented on a gray scale, display the highest concentration of the specified element as white.

Note the similarity of the gray areas on the Al and Si maps. These correspond to the similar Al and Si stoichiometries of K-spar and albite. The K map depicts K-spar as a rim around a black (no K) albite core. The size of the K-spar rims depends on the size of the albite cores. The smaller the albite core, the wider the K-spar rim, as observed by Rubin (1987) and O'Neill (2017).

#### 3.4.2.1 Potassium Feldspar

PC 1 shows the highest values for potassium, aluminum, and silicon, which corresponds to potassium feldspar (K-spar),  $\text{KAlSi}_3\text{O}_8$ . The K map has a close association with rubidium (Rb) for all 7 RT samples. Monovalent rubidium, an alkali metal, commonly substitutes for its alkali neighbor potassium in the K-spar structure. With respect to the RGB (Fig. 3.2) the pink outlines the location of K-spar, which in our analyses comprises roughly 41-56% of the rhyolite (Table 3.1), consistent with earlier studies.

### 3.4.2.2 Quartz

PC 2 shows a peak high value of silicon, which corresponds to the mineral quartz,  $\text{SiO}_2$ , for 6 out of 7 RT samples. Figs. 3.2, 3.3, and 3.4 depict the quartz grains in green. Quartz makes up approximately 16-28% of the composition of the rhyolite (Table 3.1, all filters), a range that some values lower those than in prior estimates.

### 3.4.2.3 Albite

PC 3 also displays high values for silicon, followed by aluminum and sodium (albite- $\text{NaAlSi}_3\text{O}_8$ ). Albite phenocrysts are located in blue within the RGB map. Albite ranges between 8 and 23% (Table 3.1), consistent with earlier works.

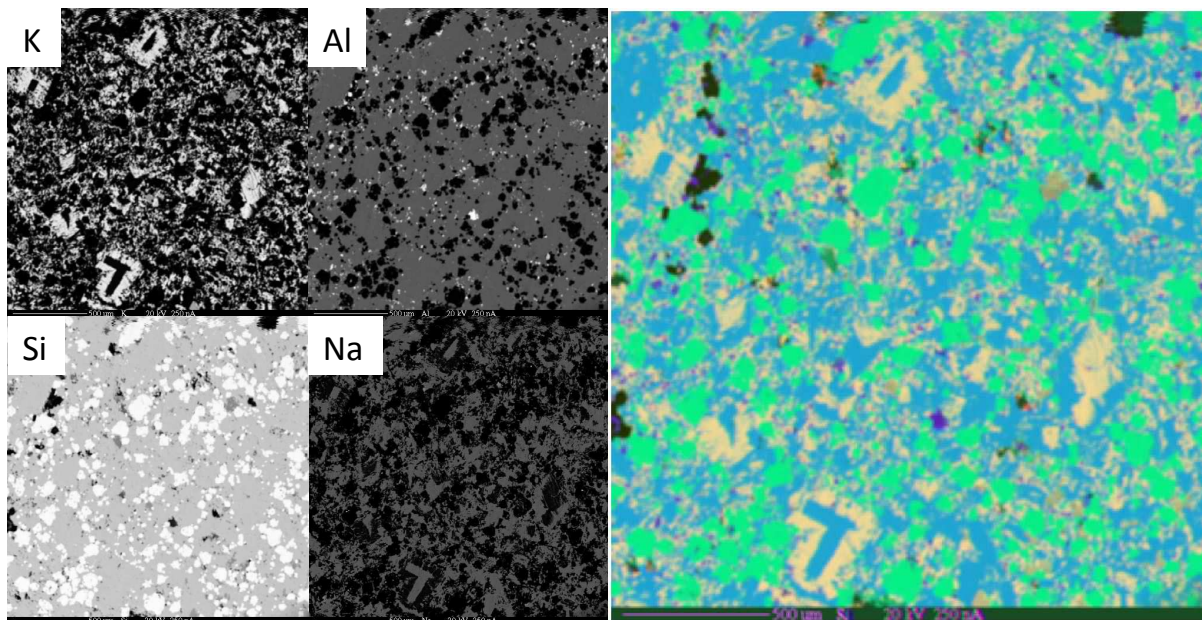


**Figure 3.2.** Top, left to right: X-ray maps of K and Al. Bottom, left to right: X-ray maps of Si and Na in the same area of the petrographic thin section of sample (RT 4) of Round Top

Mountain. Far right: RGB map of first 3 principal components (R = K-spar, G = Quartz, B = Albite). FOV 2 x 2 mm.

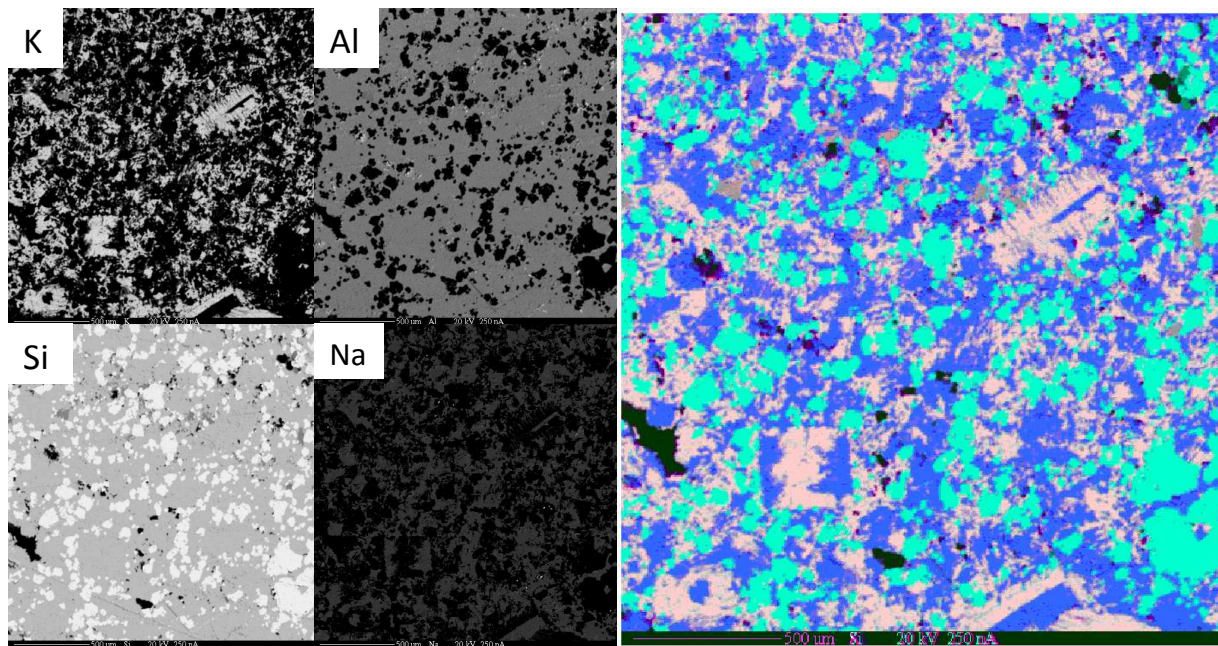


**Figure 3.3.** Top, left to right: X-ray maps of K and Al. Bottom, left to right: X-ray maps of Si and Na in the same area of the petrographic thin section of sample (RT 7) of Round Top Mountain. Far Right: RGB map of first 3 principal components (R = K-spar, G = Quartz, B = Albite). FOV 2 x 2 mm.

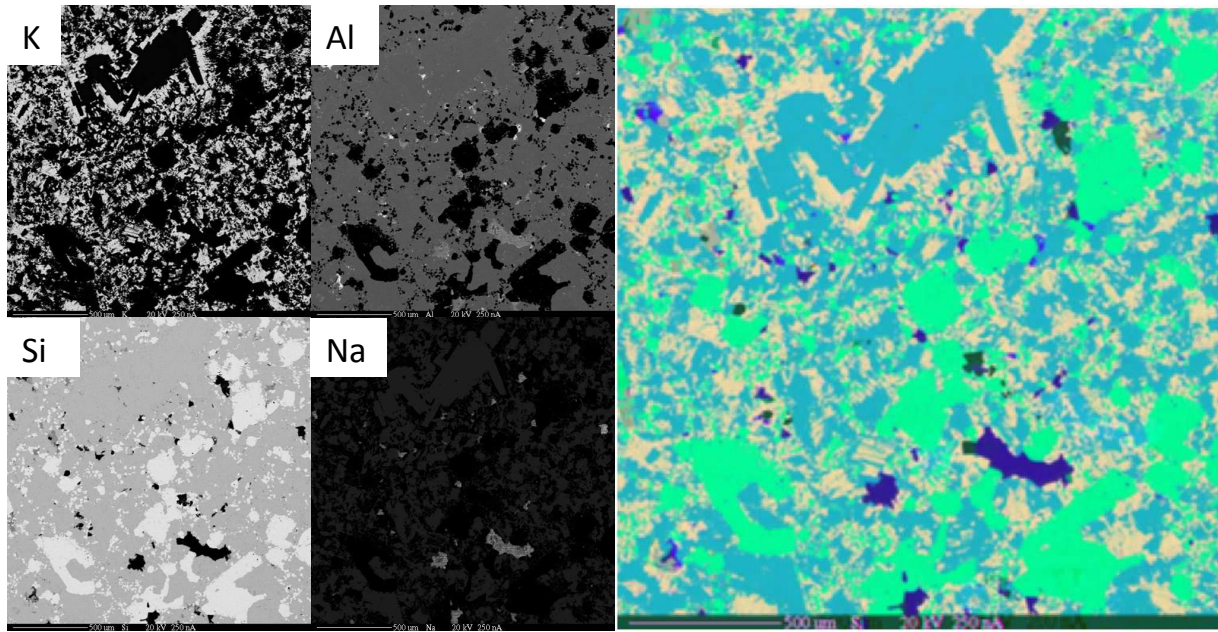


**Figure 3.4.** Top, left to right: X-ray maps of K and Al. Bottom, left to right: X-ray maps of Si and Na in the same area of the petrographic thin section of sample (RT 9) of Round Top Mountain. Far right: RGB map of first 3 principal components (R = K-spar, G = Quartz, B = Albite). FOV 2 x 2 mm.

### 3.4.3 Principal Components: Minor and Accessory Minerals

The minor minerals annite mica, magnetite, and zircon comprise 7-10% of the rhyolite. The accessory minerals yttrifluorite, columbite, thorite, and cassiterite are seen in all 7 samples in trace amounts.

#### 3.4.3.1 Annite mica

Annite mica corresponds to high loadings for Fe, Si, and Al with minor loadings of Dy (an EPMA artifact due to an overlap of X-ray emissions with Fe), F, U and Yb. The Fe map has gray shades that align well with Al and Si, consistent with the composition of an Fe-rich biotite,

annite ( $\text{KFe}_{32}\text{AlSi}_{30}\text{O}_{10}(\text{OH}, \text{F})_2$ , monoclinic). The mica found within the thin sections ranges between 1.5 and 7.9%.

### **3.4.3.2 Magnetite**

The brightest areas on the EPMA Fe X-ray maps are assumed to be magnetite ( $\text{Fe}_3\text{O}_4$ , isometric), and possibly some hematite. Magnetite percentages fall within the range from 1 to 4.8% in the rhyolite samples. Table 3.2 shows that magnetite falls between the 6th and 7th PCs.

### **3.4.3.3 Yttrifluorite**

The rare earth elements (REEs) yttrium, ytterbium, and dysprosium are among the high value economic target elements in the Round Top Mountain deposit. Dy, Y, and Yb grains correspond with one another and are incorporated in yttrifluorite. The target mineral yttrifluorite (YF), the most valuable mineral in the deposit, is present in very small amounts. Yttrifluorite ( $\text{Ca}, \text{Y}, \text{HREE})\text{F}_2$ , isometric) is a variety of fluorite ( $\text{CaF}_2$ , isometric) where up to approximately 30% of the  $\text{Ca}^{2+}$  is substituted for by Y and other mostly HREEs. Yttrifluorite ranges from 0.1 to 1.7%.

### **3.4.3.4 Zircon**

One of the minor minerals that shows up as a principal component describes where zirconium (Zr) and silicon (Si) have the highest loadings. These elements combined, as minerals, define the mineral zircon ( $\text{Zr}(\text{SiO}_4)$ , tetragonal) This PC shows up with trace amounts from 0.3 to 1.5%.

#### **3.4.3.5 Cryolite**

The 7<sup>th</sup> and 8<sup>th</sup> principal component consistently displays high loadings for sodium (Na), fluorine (F), and aluminum (Al). These elements combined, as a mineral, describe the mineral cryolite ( $\text{Na}_3\text{AlF}_6$ , monoclinic). The mineral percent composition for cryolite ranges from 0.01 to 1.9%.

#### **3.4.3.6 Columbite**

One of the accessory minerals that shows up as a principal component in high loadings for niobium (Nb), ytterbium (Yb), and iron (Fe). These elements together, as an oxide, describe the mineral columbite ( $\text{Fe}^{2+}\text{Nb}_2\text{O}_6$  to  $\text{Mn}^{2+}\text{Nb}_2\text{O}_6$ , orthorhombic). Columbite mineral percentage present between the 7 samples ranges from 0.1 to 1.1%.

#### **3.4.3.7 Thorite**

The 14<sup>th</sup> principal component is consistently displays high loadings for thorium (Th), uranium (U), and silicon (Si). These elements combined, as a mineral, describe the mineral thorite ( $\text{Th}(\text{SiO}_4)$ , tetragonal). The mineral percent composition for thorite ranges from 0.1 to 0.4%.

#### **3.4.3.8 Uraninite**

The 15<sup>th</sup> principal component is consistently displays high loadings for uranium (U). This element combined with oxygen, as a mineral, describes the mineral uraninite ( $\text{UO}_2$ , isometric). The mineral percent composition for uraninite ranges from 0.01 to 0.12%.



### **3.4.3.9 Cassiterite**

Another accessory mineral displays high loadings for tin (Sn). This element, as an oxide, describes the mineral cassiterite ( $\text{SnO}_2$ , tetragonal). The mineral percent composition for cassiterite ranges from 0.02 to 0.9%.

### **3.4.4 Mineral Maps**

The following maps were produced by application of PCA to two separate thin sections. These mineral maps show the spatial distribution of each of the three major minerals: potassium feldspar, quartz, and albite. The minimal percent difference between the mineral maps is consistent with other evidence (Pingitore et al., 2018a) for a homogenous deposit. It also corroborates the results found in previous articles regarding the range in percentages of major and minor minerals, including minerals of economic importance such as yttrifluorite. Fig. 5 presents maps of samples RT 2 and RT 12. The K-spar (pink) phenocrysts found in these two samples range in size between 50 and 250  $\mu\text{m}$  in length. The K-spar surrounds the albite cores (light gray) as rims; the albite ranges from 20 to 100  $\mu\text{m}$  in length. The location of the quartz is indicated in yellow and is seen dispersed randomly throughout the thin sections. The quartz grains range from 20 to 150  $\mu\text{m}$  and are anhedral to subhedral in appearance. Magnetite (black) and annite biotite (brown) are both found dispersed randomly throughout, with phenocrysts ranging between 10 and 100  $\mu\text{m}$  in length. There is also the presence of minor or accessory minerals such as zircon, cryolite, yttrifluorite, cassiterite, columbite, uraninite and thorite although these minerals are so few and mostly found in trace amounts they are not depicted here.

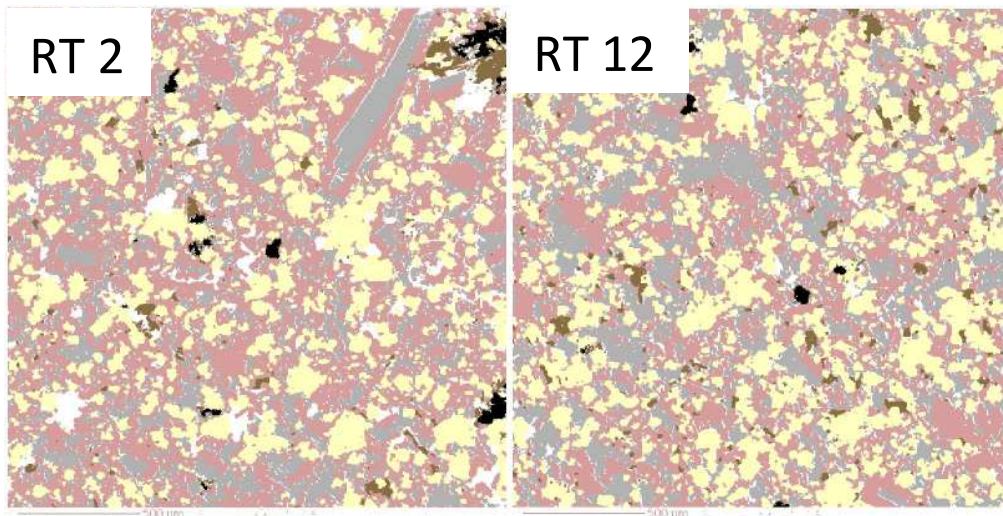


**Figure 3.5.** Mineral maps of thin sections of samples RT 7 and RT 10. K-spar (pink), albite (light gray), quartz (yellow), magnetite (black), annite mica (brown) FOV 2 x 2 mm.

### 3.4.5 Comparison of results with previous studies

Table 3 is a comparison of our computer-generated compositions (averages of 7 samples) compared to results in earlier studies. This is a test, albeit an imperfect one, or “ground-truthing” of our technique. Note that the earlier studies employed several different analytic techniques. More importantly, most of these studies collected surface samples from the deposit. These might have been altered by proximity to country rock during emplacement of the laccolith or been subjected to weathering in their surficial environment. Our samples were from drill cuttings and likely are more representative of the actual bulk of the deposit.

The QEMSCAN™ (one sample) and RT ALS (composited drill cutting samples) analyses were provided by Texas Mineral Resources Corp. QEMSCAN™ employs an SEM with EDS detectors and attempts to match the X-ray energy spectrum recorded at each pixel to a catalog of known mineral spectra. With the exception of the results of this study and the QEMSCAN™, all entries are mathematically derived conventional petrological CIPW element-

to-mineral conversions of the bulk elemental analyses in those respective studies (CIPW norm calculator, 2019).

As anticipated, there is general agreement among these studies, suggesting that our approach is valid. Again, we emphasize that the actual overall composition of the laccolith is both unknown and unknowable, and all attempts to characterize that composition are limited by sampling and analytical considerations.

**Table 3.3.** Comparison of Round Top Mountain CIPW norm mineral compositions among authors.

Authors Technique	This Study EPMA + ArcGIS		QEMSCAN SEM-EDS		RT ALS ICP-MS		Rubin 1987 Bureau of Econ Geo ICP-AES		Price 1990 ICP-MS		Shannon 1986 INAA		O'Neill 2014 ICP-AES/MS		O'Neill 2014 Optical Estimated		O'Neill 2017 ICP-MS	
	Wt % Norm	Vol % Norm	Wt % Norm	Vol % Norm	Wt % Norm	Vol % Norm	Wt % Norm	Vol % Norm	Wt % Norm	Vol % Norm	Wt % Norm	Vol % Norm	Wt % Norm	Vol % Norm	Wt % Norm	Vol % Norm	Wt % Norm	Vol % Norm
Minerals																		
Quartz	25.8	26.2	27.6	28.1	25.8	25.5	21.6	21.3	21.8	21.2	27.6	28.7	29.8	30.1	29.0	29.0	28.9	29.1
Plagioclase	38.6	39.9	30.7	31.7	46.3	46.3	46.9	46.7	47.0	46.1	40.9	43.2	40.8	41.6	10.9	11.0	41.0	41.7
Orthoclase	24.6	25.8	30.8	32.3	23.7	24.2	24.9	25.4	24.9	25.0	23.6	25.4	25.3	26.4	48.6	50.0	25.2	26.3
Corundum											0.12	0.08	0.75	0.50			1.01	0.67
Hypersthene					0.15	0.12	1.41	0.93	2.58	1.68	2.58	2.01	0.17	0.15			0.22	0.19
Acmite					1.37	0.99	2.08	1.51										
Na <sub>2</sub> SiO <sub>3</sub>							1.30	1.42	1.83	1.96								
Ilmenite					0.04	0.02	0.04	0.02	0.06	0.03	0.02	0.01	0.04	0.02			0.04	0.02
Magnetite	4.04	2.10	0.90	0.47	0.19	0.09					1.15	0.61	2.07	1.06	5.87	3.00	1.88	0.96
Hematite					1.00	0.50							0.17	0.09			0.24	0.12
Apatite					0.05	0.04	0.02	0.02	0.02	0.02			0.02	0.02			0.05	0.04
Zircon	0.58	0.33	0.27	0.15	0.19	0.11	0.21	0.12	0.22	0.13			0.21	0.12			0.21	0.12
Chromite					0.01	0.01												
Fluorite			0.70	0.60	2.45	2.01	3.22	2.64	4.80	3.88							0.96	0.81
Yttrifluorite	0.12		0.06	0.05														
Columbite	0.40		0.09	0.01														
Cassiterite	0.34		0.03	0.04														
Thorite	0.15		0.07	0.04														
Mica (Annite)	4.21		4.90	4.40											5.67	5.00		
Cryolite	0.58		1.80	1.64														
Uraninite	0.58																	
Bast or cer			0.01	0.01														
Xenotime																		
Monazite																		
Carbonate			0.20	0.20														
Gearsutite			0.20	0.19														
Thomsenolite																		
Ralstonite			0.10	0.10														

### **3.4.6 Mineralogical textural analysis: Yttrifluorite distribution**

To discern which minerals neighbor the valuable target yttrifluorite we overlay the YF map on top of the maps containing the major and minor minerals (Figure 6). Zooming into individual YF grains, approximately 1-20  $\mu\text{m}$  in length, those neighbors could be determined. Six out of the seven mineral maps showed that the majority of the YF grains were associated with K-spar and quartz grains. Occasionally, the YF grains abut albite grains and, less commonly, the iron-rich phases, magnetite or annite mica. Round Top samples RT 2, RT 4, RT 7, RT8, RT 9 and RT 12 primarily coincide with both feldspars (K-spar and albite) that lie near quartz grains. RT 10 exhibited a different behavior where the YF grains are solely found on the Fe-rich mica (annite).

We had expected that perhaps the YF would be clustered adjacent to, or in micro-pods with, other minerals containing incompatible elements that were precipitated contemporaneously with the YF in the late-stage fluorine mineralization event. This does not appear always to have been the case, with some of the yttrifluorite isolated from, and some associated with the minor and accessory minerals. Concentration concentration of the valuable YF with such other potential targets as columbite-tantalite, cassiterite, zircon, and uraninite would have suggested that fine grinding and mechanical separation of such clusters could be an economically viable approach to exploiting this multi-mineral deposit.

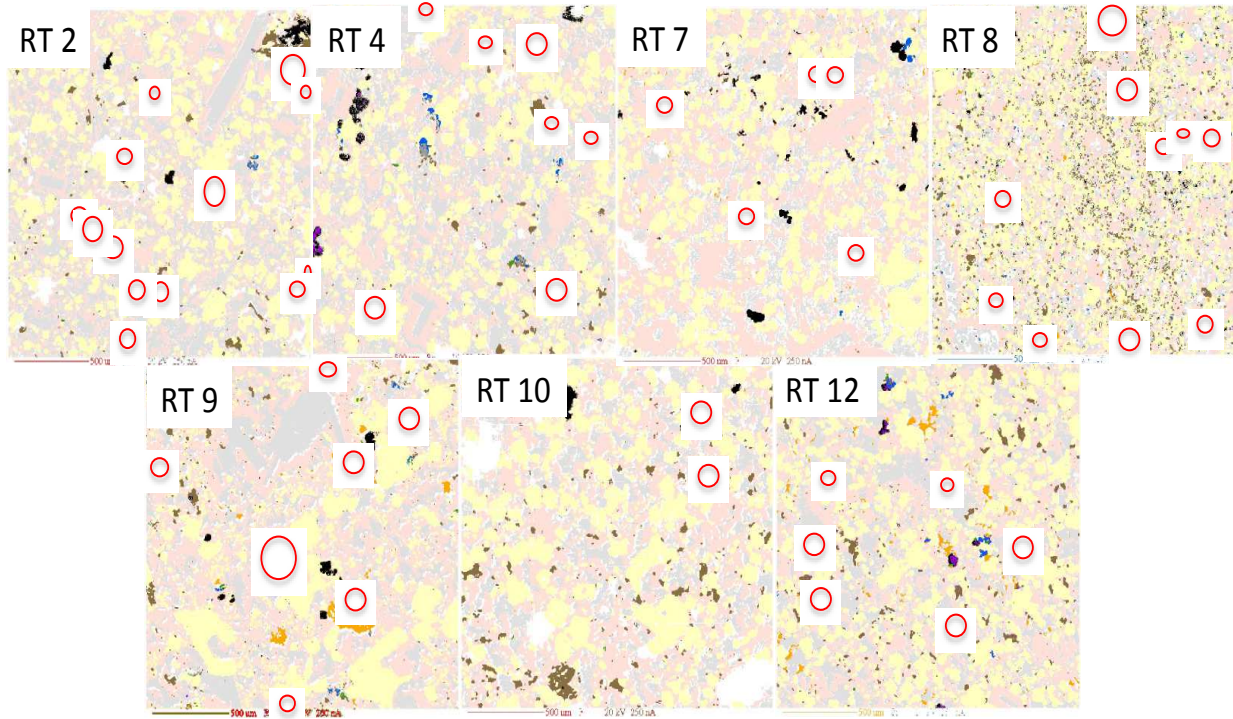


**Figure 3.6.** Mineral maps of all 7 RT maps with major minerals, K-spar (pink), albite (10% gray), quartz (yellow); minor minerals, magnetite (black), annite mica (brown) and accessory minerals zircon (blue), cryolite (orange), uraninite (40% gray), thorite (purple), cassiterite (light blue), columbite (green), and yttrifluorite (red and circled). FOV 2 x 2 mm.

### 3.4.7 Petrophysical analysis: Porosity

Previous studies have shown that Round Top Mountain rhyolites have 1 to 2% porosity in the gray varieties and 3-8% porosity in the pink varieties (Negrón et al., 2016). This porosity is evident in the mineral maps. Fig. 3.7 shows sample RT, with a pulled out section of the upper right-hand corner enlarged in order to highlight this porosity. The black areas are the pore spaces found between minerals. Each pixel is approximately 2  $\mu\text{m}$  in size. Using ArcGIS™, the percentage of pore spaces was calculated to range from 1.4 to 4.0 % in the 7 samples, consistent with earlier measurements of porosity by water saturation (Negrón et al., 2016).

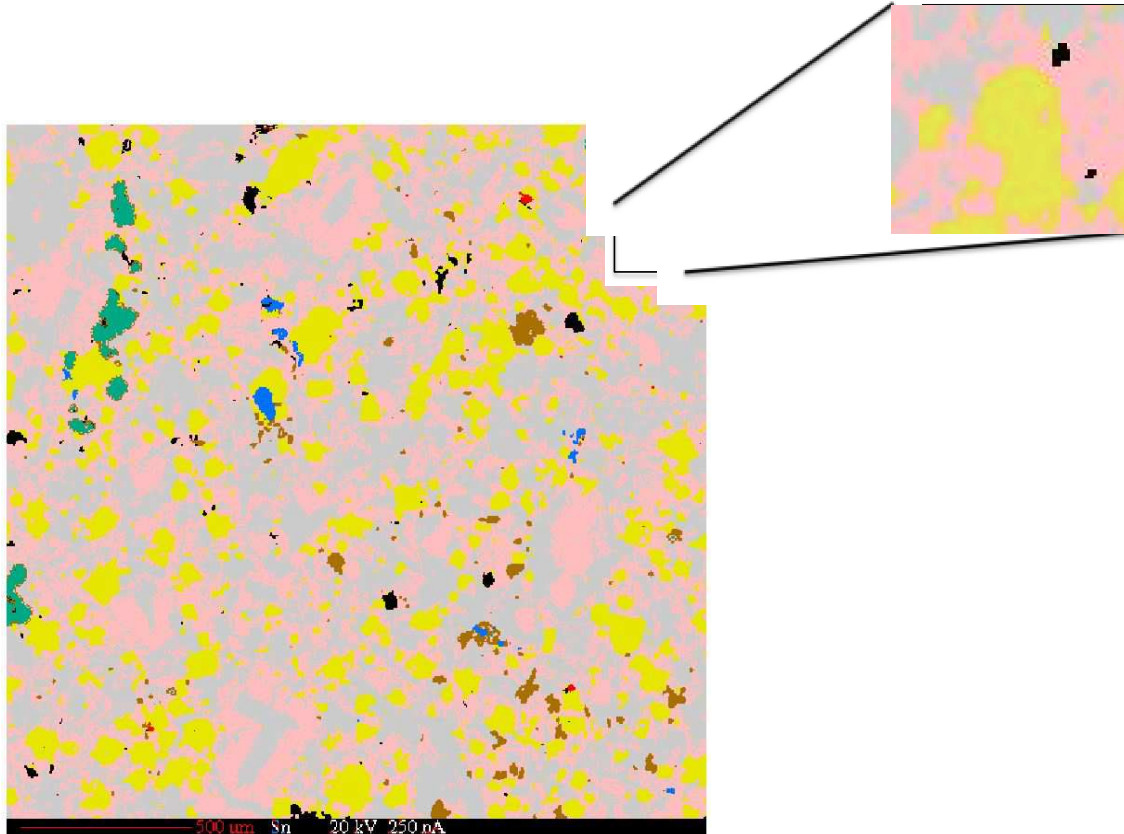


**Figure 3.7.** Mineral map of sample RT 4 showing pore space (black areas). FOV 2 x 2 mm.

### 3.5 CONCLUSION

Multivariate analysis was performed on seven thin sections of Round Top Mountain rhyolite. Through the use of the XRMA tool package in ArcGIS™, principal components were derived and percentages of major and minor minerals were determined. By overlaying the X-ray element maps in ArcGIS™, element-mineral correlations were observed for each principal component at each pixel. This enabled conversion of the elemental maps into mineral maps. Resulting overall mineralogy proved consistent with results from prior investigations. This new approach presents the opportunity to use computer-generated information to provide an unbiased basis for creation of mineralogical maps from elemental maps.

## ACKNOWLEDGEMENTS

The authors thank Texas Mineral Resources Corporation for providing access to proprietary technical data and samples. This project was supported by joint research contracts 26-8211-12 and 26-8211-16 between TMRC and the University of Texas at El Paso. Funds to cover the costs to publish in open access were obtained from this source. Also, we thank Prof. Gaetano Ortolano and Ph.D candidate Roberto Visalli from the University of Catania, Italy for access to their X-ray Map Analyzer application.

## References

Audet, R.H. and Abegg, G.L. (1996) Geographic Information Systems: Implications for Problem Solving. *Journal of Research in Science Teaching*, **33**(1), 21-45.

[https://doi.org/10.1002/\(SICI\)1098-2736\(199601\)33:1<21::AID-TEA2>3.0.CO;2-R](https://doi.org/10.1002/(SICI)1098-2736(199601)33:1<21::AID-TEA2>3.0.CO;2-R)

Borůvka, L., Vacek, O., and Jehlička. (2005) Principal component analysis as a tool to indicate the origins of potentially toxic elements in soils. *Geoderma*, **128**, 289-300

Chatterjee, N. (2012) Electron Microprobe Analysis. MIT Course 12.141 Notes

CIPW norm calculator. <https://www.geologynet.com/programs/cipwnormexcel.xls>

Crósta, A.P., De Souza Filho, C.R., Azevedo, F., and Brodie, C. (2003) Targeting key alteration minerals in epithermal deposits in Patagonia, Argentina, using ASTER imagery and principal component analysis. *International Journal of Remote Sensing*, **24**(21), 4233-4240



Dostal, J. (2017) Rare Earth Element Deposits of Alkaline Igneous Rocks. *Resources*, **6**(34), doi:10.3990/resources6030034

Elliott, B.A., O'Neill, L.C. and Kyle, J.R. (2017) Mineralogy and Crystallization History of a Highly Differentiated REE-Enriched Hypabyssal Rhyolite: Round Top Laccolith, Trans-Pecos, Texas. *Mineralogy and Petrology*, **111**, 569-592

Gasser, R., Knežević, G., Carrier, M. (2015) Mine Risk Management by Mapping. *Journal of ERW and Mine Action*, **15**(2), Article 21

Gustavson Associates. (2013) NI 43-101 Preliminary Economic Assessment: Round Top Project, Sierra Blanca, Texas. [http://tmrcorp.com/news/technical\\_reports/](http://tmrcorp.com/news/technical_reports/)

Jowitt, S.M., Medlin, C.C. and Cas, R.A.F. (2017) The Rare Earth Element (REE) Mineralisation Potential of Highly Fractionated Rhyolites: A Potential Low-Grade, Bulk Tonnage Source of Critical Metals. *Ore Geology Reviews*, **86**, 548-562. <https://doi.org/10.1016/j.oregeorev.2017.02>

Khashgerel, B., Kavalieris, I. & Hayashi, K. (2008) Mineralogy, textures, and whole-rock geochemistry of advanced argillic alteration: Hugo Dummett porphyry Cu-Au deposit, Oyu Tolgoi mineral district, Mongolia. *Mineralium Deposita*, **43**(8), 913-932. DOI 10.1007/s00126-008-0205-3

Malehmir, A., Durrheim, R., Bellefleur, G., Urosevic, M., Juhlin, C., White, D.J., Milkereit, B., Campbell, G. (2012) Seismic methods in mineral exploration and mine planning: A general overview of past and present case histories and a look into the future. *Geophysics*, **77**(5), WC173-WC190

McLemore, V. T. (2018) Rare Earth Elements (REE) Deposits Associated with Great Plain Margin Deposits (Alkaline-Related) Southwestern United States and Eastern Mexico. *Resources*, **7**(8), doi:10.3390/resources7010008

Negrón, L., Pingitore Jr., N.E., Gorski, D. (2016) Porosity and Permeability of Round Top Rhyolite (Texas, USA) Favor Coarse Crush Size for Rare Earth Element Heap Leach. *Minerals*, **6**(1), 16; DOI:10.3390/min6010016. <http://www.mdpi.com/2075-163X/6/1/16>

O'Neill, LC. (2014) REE-Be-U-F mineralization of the Round Top laccolith, Sierra Blanca peaks, Trans-Pecos Texas. MSc thesis, University of Texas at Austin.

O'Neill, L.C., Elliott, B.A., and Kyle, J.R. (2017) Mineralogy and crystallization history of a highly differentiated REE-enriched hypabyssal rhyolite: Round Top laccolith, Trans-Pecos, Texas. *Mineralogy and Petrology*, **111**, 569-592. DOI 10.1007/s00710-017-0511-5

Ortolano, G., Zappalà, L., Mazzoleni, P. (2014) X-ray Map Analyser: A new ArcGIS™® based tool for the

quantitative statistical data handling of X-ray maps (Geo- and material-science applications).

*Computers & Geosciences*, **72**, 49-64. <https://doi.org/10.1016/j.cageo.2014.07.006>

Percentage by weight to percentage by volume conversion calculator.

<https://www.handymath.com/cgi-bin/dnstywtvol.cgi?submit=Entry>

Petrash, D.A, Gingras, M.K., Lalonde, S.V., Orange, F., Konhauser, K.O. (2012) Dynamic controls on accretion and lithification of modern gypsum-dominated thrombolites, Los Roques, Venezuela. *Sedimentary Geology*, **245-246**, 29-47

Pingitore Jr. N.E., Clague, J.W., and Gorski, D. Round Top Mountain (Texas, USA) a Massive, Unique Y-bearing-fluorite-hosted Heavy Rare Earth Element (HREE) Deposit. 2012. *Journal of Rare Earths*, **32**, 90-96. [https://doi.org/10.1016/S1002-0721\(14\)60037-5](https://doi.org/10.1016/S1002-0721(14)60037-5)

Pingitore Jr., N.E., Clague J.W., Gorski, D. (2018a) Remarkably consistent rare earth element grades at Round Top yttrifluorite deposit. *Advances in Materials Physics and Chemistry, Special Issue: Rare Earth Elements*, **8**(1),1-14. DOI: 10.4236/ampc.2018.81001

Pingitore Jr., N.E., Piranian, M., Negrón, L., Gorski, D. (2018bf) Microprobe Mapping of Rare Earth Element Distribution in Round Top Yttrifluorite Deposit. *Advances in Materials Physics and Chemistry, Special Issue* **8**(1), 15-31. DOI: 10.4236/ampc.2018.81002  
<https://doi.org/10.4236/ampc.2018.81002>

Price, J.G, Rubin J.N., Henry, C.D., Pinkston, T.L., Tweedy, S.W., Koppenaar, D.W. (1990) Rare-metal enriched peraluminous rhyolites in a continental arc, Sierra Blanca area, Trans-Pecos Texas; chemical modification by vapor-phase crystallization. *GSA Special Papers* **246**, 103-120. <http://dx.doi.org/10.1130/SPE246-p103>

Price, M.H. (2016) *Mastering ArcGIS™*. McGraw Hill Education. Seventh Edition.

Rambert, F. (2005) Introduction to Mining Geostatistics. *67<sup>th</sup> EAGE Conference and Exhibition*, DOI: [10.3997/2214-4609.201405201](https://doi.org/10.3997/2214-4609.201405201)

Rubin, J.N., Price, J.G., Henry, C.D. and Koppenaar, D.W. (1987) Cryolite-Bearing and Rare Metal-Enriched Rhyolite, Sierra Blanca Peaks, Hudspeth County, Texas. *American Mineralogist*, **72**, 1122-1130

Shannon, W.M (1986) Lithogeochemical characterization of intrusive rocks comprising the Quitman-Sierra Blanca igneous complex, Hudspeth County, Texas. M.S. thesis, University of Texas at El Paso

Sprague, K., de Kemp, E., Wong, W., McGaughey, J., Perron, G., Tucker, B. (2006) Spatial targeting using queries in a 3-D GIS environment with application to mineral exploration. *Computers & Geosciences*, **32** (3), 396-418. <https://doi.org/10.1016/j.cageo.2005.07.008>

## **Chapter 4: ArcGIS™ Proximity and Cluster Analysis of Electron Probe**

### **Micromaps of Round Top Critical Mineral Deposit**

#### **4.1 ABSTRACT**

Critical and rare earth elements are in high demand for their application in technological devices, including those required for the transition to green energy. Round Top Mountain rhyolite, a laccolith in Sierra Blanca, West Texas, is a unique mineral deposit that offers opportunity for development of rare earth elements, especially the heavy rare earths, as well as associated critical elements. The main objective here is to evaluate the distances between accessory minerals of potential economic value (yttrifluorite, cryolite, uraninite, thorite, cassiterite and columbite) to major (potassium feldspar, albite and quartz) and minor minerals (annite mica, magnetite and zircon). In this study we explore the proximity and clustering of these minor and accessory minerals, at the micron scale from mineral maps constructed in a previous application of ArcGIS™ tools to superimposed electron probe microanalysis (EPMA) x-ray element maps. Our goal is to determine whether specific minerals cluster spatially and, if so, at what distances. We noted that the high-value target yttrifluorite grains often neighbor potassium feldspar and quartz grains, as well as magnetite and mica grains. With regards to cluster analysis, most minor and accessory minerals were found to cluster at small scales and were dispersed or random at larger distances.

#### **4.2 INTRODUCTION**

In this study, we examine minor and accessory minerals from a potentially economically

valuable deposit of heavy rare earth elements (HREEs) and other critical elements (Rubin et al., 1987; Price et al., 1990; Pingitore et al., 2012; O'Neill et al., 2014; Negrón et al., 2016; O'Neill et al., 2017; Pingitore et al., 2018a). Round Top Mountain is a rhyolite laccolith in Hudspeth County, west Texas, U.S.A. This Tertiary mushroom-shaped, peraluminous igneous intrusion has a mass estimated at 1.6 billion tons, and is approximately 2000 m in diameter and over 375 m in height. The major elemental composition of the rhyolite comprises Si, O, K, Al, and Na. This unique deposit underwent chemical alteration by a late-stage fluorine vapor phase that enriched it in HREEs and other incompatible elements (Price et al., 1990; Gustavson Associates, 2013; O'Neill et al., 2017). The laccolith exhibits exceptionally homogeneous mineralization (Pingitore et al., 2018a), with a rare earth element (REE) concentration over 500 ppm, of which the desirable yttrium + HREEs (YHREEs) comprise approximately 72%, making it of global significance (Pingitore et al., 2012; Negron et al., 2016).

This research is an extension of previous works on the Round Top Mountain deposit (Pingitore et al., 2018b; Negron et al., 2019) in which electron microprobe elemental maps and multivariate statistical analysis (principal component analysis) were used to create mineralogical maps. In this paper, those mineral maps are further analyzed spatially through proximity and cluster analyses using tools in the ArcGIS™ software system. The purpose of this study is to ascertain whether specific minerals of potential economic value are clustered or dispersed at the millimeter and lower scale in the rhyolite. This information can aid in understanding the formation and possible extraction of the target critical elements.

Multivariate spatial cluster analysis using ArcGIS™ has been widely applied in a variety of fields (Lee & Song, 2007; Zhang et al., 2010; Anju & Banerjee, 2012; Ma et al., 2015). Here proximity analysis would evaluate the separation between yttrifluorite grains, and their

proximity to other minor minerals. Cluster analysis would demonstrate whether minor and accessory minerals exhibit clustering patterns and if so, at what distance or distance ranges. This approach employs Ripley's K function to show how spatial clustering or dispersion of feature centroids changes as neighborhood sizes increase.

## **4.3 METHODS**

### **4.3.1 Sample collection and preparation**

Composite samples were obtained from reverse circulation drilling of Round Top Mountain rhyolite by Texas Mineral Resources Corporation, a publicly traded (stock ticker TMRC) junior mining explorer. TMRC is interested in testing this area and evaluating the mineralization in the rhyolite. Random sample pieces were chosen and thin sections were made by mounting pieces to a surface, ground flat, glued to a petrographic glass slide and polished to a mirror finish (Pingitore et al., 2017).

### **4.3.2 Electron probe microanalysis**

Four thin sections were analyzed for 16 elements: Al, Ca, Dy, F, Fe, K, Na, Nb, Rb, Si, Sn, Th, U, Yb, Y, Zr, using an electron probe micro-analyzer (EPMA). This technique determines elemental compositions of individual grains or portions of grains in thin sections *via* a beam of accelerated electrons focused on a micrometer-sized site. The beam of electrons interacts with the electrons of the elements and causes emission of characteristic X-rays of those elements (Khashgerel et al., 2008). The EPMA used was a Cameca SX-50 (upgraded to SX-100 performance) with 4 wavelength dispersive spectrometers (WDS). Each randomly selected 2 x 2 mm area was WDS raster scanned repeatedly to yield 516 x 516 pixel elemental maps. The

quality of the X-ray images depends on several factors including: the particular element, its concentration, dwell time of the beam on each pixel, and the beam current. Instrument settings were 20 KeV accelerating electron beam voltage and 200 or 250 nA current.

#### **4.3.3 ArcGIS™ – Proximity Analysis**

The first analysis determined the distances between each of the yttrifluorite (YF) grains in a map. One approach is to create buffers to surround each YF grain to assist in measuring the proximity between grains using feature classes. The buffer tool works by creating a buffer (ring) polygon at a user specified distance. There are two types of buffers: Euclidean and geodesic. Due to the nature of our dataset and the custom reference frame we created, we used the Euclidean buffer that measures in a two-dimensional Cartesian plane. The planar method suited our data and buffer distances of 1-, 10-, and 100- $\mu\text{m}$  were tried. However, the use of the 1- and 10- $\mu\text{m}$  buffer distances proved appropriate to the small size of the yttrifluorite grains (Figure 4.1).

#### **4.3.4 ArcGIS™ – Cluster Analysis**

The ArcGIS™ raster calculator tool created separate mineral maps by overlapping multiple individual element X-ray maps and correlating the pixels in which elements of a specific mineral occur together. These individual mineral maps were then converted from rasters to feature classes in order to use geo-processing spatial analysis tools. The feature classes are further studied through the use of Multi-Distance Spatial Cluster Analysis (Ripley's K-function). This tool determines whether features exhibit statistically significant clustering or dispersion over a range of distances and requires 'projected data' to accurately measure distances (Mitchell, 2005).



We created a custom projection of 2000  $\mu\text{m}$  by 2000  $\mu\text{m}$  using the Data Management toolbox and defining our own projection.

To ensure high-level statistical significance we used the 99.9% confidence interval (CI) for the smaller datasets and the 90% CI and 99% CI for larger datasets. The confidence level/interval depends on the number of permutations the user chooses. For example, 9 permutations are required for the 90%, 99 permutations for 99% and 999 permutations for 99.9%. The permutations refer to the number of randomly placed points in the study area that is equal to the number of points in the feature class. The set of points, permutations, are distributed that many times (9, 99, 999) per iteration. The majority of the data reasonably fit within a distance of 300  $\mu\text{m}$  for all minerals and all samples using 99 permutations (99% CI) and 999 permutations (99.9% CI).

A total of 60 distance bands were generated with a beginning distance of 5  $\mu\text{m}$ , increasing by increments of 5  $\mu\text{m}$  per iteration of the analysis. We also used the Ripley's Edge Correction Formula for square and rectangular data because it checks each point's distance from the edge of the study area and its distance to each of its neighbors (Mitchell, 2005). To be considered statistically significant, the observed K-values must be above the higher confidence interval (clustering) or below the lower confidence interval (dispersion). K-values that fall between the confidence intervals and along the expected K-value line reflect a random distribution of the item of interest.

## 4.4 RESULTS AND DISCUSSION

### 4.4.1 Proximity analysis of yttrifluorite

Yttrifluorite (YF) is a variety of fluorite ( $\text{CaF}_2$ , isometric) in which yttrium and REEs, particularly HREEs, substitute for up to some 30% of the Ca (mindat, 2019). Because virtually all of the YHREEs at Round Top are hosted in YF (Pingitore et al., 2012), it is the target mineral for REE extraction. Map RT 8 has the largest number of yttrifluorite grains of the 4 maps studied (Table 4.1). The longest distance between yttrifluorite grains is 2000  $\mu\text{m}$  and the shortest distance is 17  $\mu\text{m}$ . The average distance between YF grains between all four RT maps is 864  $\mu\text{m}$ . The important factor is the random dispersion of the yttrifluorite grains that possibly renders extraction of those grains by mechanical separation and concentration more difficult than if there were multiple grains in close proximity. At times the YF grains are spread randomly throughout the entire 2 x 2 mm square map, creating the large variation in distances. In contrast, when the YF grains are found segregated to a certain quadrant of the thin section, the distance between grains shortens.

The mineral neighbors of the YF grains were also identified (Table 4.1). Knowledge of the neighboring minerals can inform the ease at which the yttrifluorite might be extracted, i.e., whether the YF grains are proximal to soluble or to insoluble minerals. All samples have some YF grains that are surrounded by minerals, feldspars and quartz, that are insoluble in the dilute sulfuric acid ( $\text{H}_2\text{SO}_4$ ) that has been proposed for YF extraction by heap leaching. There also are many YF grains that are associated with Fe-bearing pixels (typically magnetite or hematite) and annite mica grains; both these neighbors are soluble in dilute sulfuric acid. This is consistent with a previous study that showed an increase in pore space after exposure to sulfuric acid, which apparently assists in the efficient extraction of the YF-hosted REEs (Negron et al., 2016).

**Table 4.1.** Number, size, and proximity of YF grains and their neighboring minerals.

Sample ID	# YF grains	Smallest Grain	Largest Grain	Shortest Distance	Longest Distance	Average Distance	Neighboring Minerals
RT 2	12 YF	2 $\mu\text{m}$	24 $\mu\text{m}$	30 $\mu\text{m}$	1600 $\mu\text{m}$	737 $\mu\text{m}$	grains associated with Al map others found next to kspar & qtz
RT 4	7 YF	2 $\mu\text{m}$	56 $\mu\text{m}$	30 $\mu\text{m}$	1925 $\mu\text{m}$	1008 $\mu\text{m}$	grains near kspar & qtz others associated with F map
RT 8	15 YF	4 $\mu\text{m}$	40 $\mu\text{m}$	150 $\mu\text{m}$	2000 $\mu\text{m}$	987 $\mu\text{m}$	primarily surround or on top of kspar grains others next to qtz
RT 12	13 YF	2 $\mu\text{m}$	16 $\mu\text{m}$	20 $\mu\text{m}$	1150 $\mu\text{m}$	723 $\mu\text{m}$	surrounded by kspar or associated with magnetite

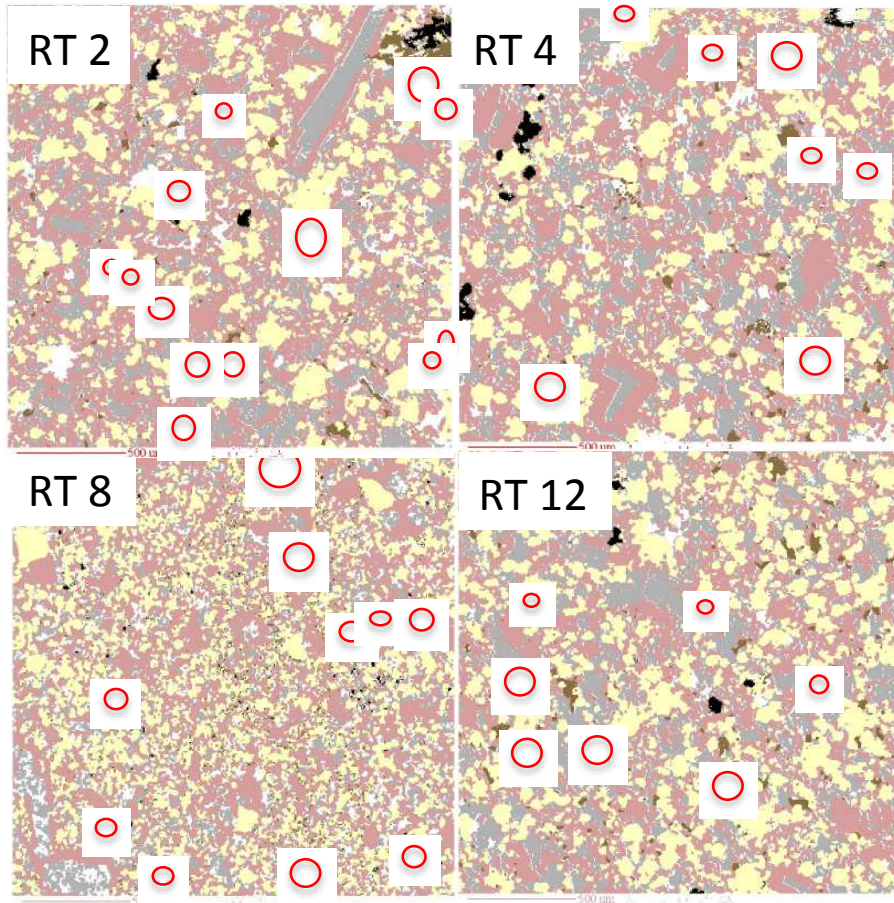


**Figure 4.1.** Mineral maps generated from electron probe microanalysis of 4 Round Top rhyolite samples. Field of view is 2 mm x 2 mm. YF grains circled in red. In some circles there are multiple yttrifluorite grains in close proximity to one another. Following colors correspond to minerals: K-spar (pink), albite (gray), quartz (yellow), magnetite (black) and annite mica (brown) and yttrifluorite (red and circled).

#### 4.4.2 Ripley's K cluster analyses

In the figures that follow (Figs. 4.2-4.10), the blue line represents the expected K-values for random distribution, red line is the observed K-values for each distance, and the dotted lines are

the upper and lower limits of the confidence envelope (99% and 99.9%). Points that fall above the expected blue line indicate clustering, but they are only significant if they are above the upper limit of the confidence envelope.

Ripley's K analysis can be sensitive to the size of the project area being evaluated and our results reflect that in part. Choosing appropriate parameters was necessary, which prevented rendering graphs whose axes reached 2000  $\mu\text{m}$ . At greater distances the confidence interval and observed k-values bent off the scale and thus were no longer valid.

#### **4.4.2.1 Magnetite ( $\text{Fe}_3\text{O}_4$ , cubic)**

Magnetite is the fourth most common mineral found in Round Top rhyolite samples. Magnetite shows statistically significant clustering in RT 2 (in the distance range of 10 to 120  $\mu\text{m}$ ) and RT 4 (5-80  $\mu\text{m}$ ) samples (Fig. 4.2). There is some clustering found in the RT 8 sample, also ranging in the range of 10-80  $\mu\text{m}$ , whereas there is no clustering at all observed in RT 12. RT 2 and RT 4 show minimal statistically significant dispersion at large distances ranging from 232-300  $\mu\text{m}$  and 242-300  $\mu\text{m}$ , but neither RT 8 nor RT 12 shows any dispersion. With the exception of RT 2 and RT 4, it is notable that some clustering occurs at short distances but the mineral magnetite appears to be more randomly distributed.

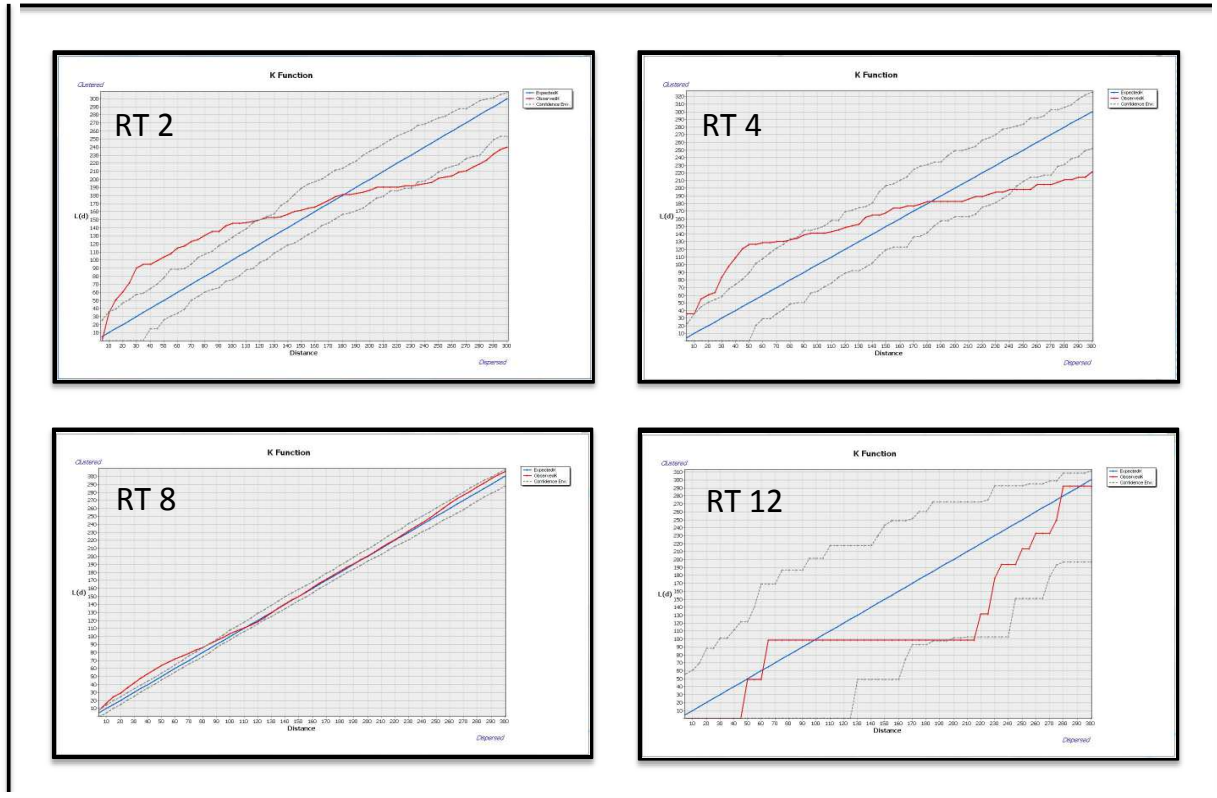


**Figure 4.2.** Cluster analysis results for magnetite. Distance (x-axis) vs. Ripley's K (y-axis). Expected K values (blue line), observed K values (red line), and confidence interval (dotted line).

#### 4.4.2.2 Annite mica ( $K(Mg, Fe)_3(AlSi_3O_{10})(F, OH)_2$ , monoclinic)

Annite mica is another common mineral found throughout Round Top rhyolite and it also displays significant short-distance clustering in RT 2 and RT 4 samples (Fig. 4.3). Their clustering ranges from 5-150  $\mu\text{m}$  and 5-205  $\mu\text{m}$ , respectively. RT 8 exhibits statistically significant clustering that spans the entire scale from 5-300  $\mu\text{m}$ . Similarly, RT 12 also shows some clustering with distances from 5-110  $\mu\text{m}$  and again between 270-300  $\mu\text{m}$ . RT 2 shows

dispersion at distances greater than 150  $\mu\text{m}$  and RT 4 at distances greater than 245  $\mu\text{m}$ . RT 8 and RT 12 do not show any dispersion.

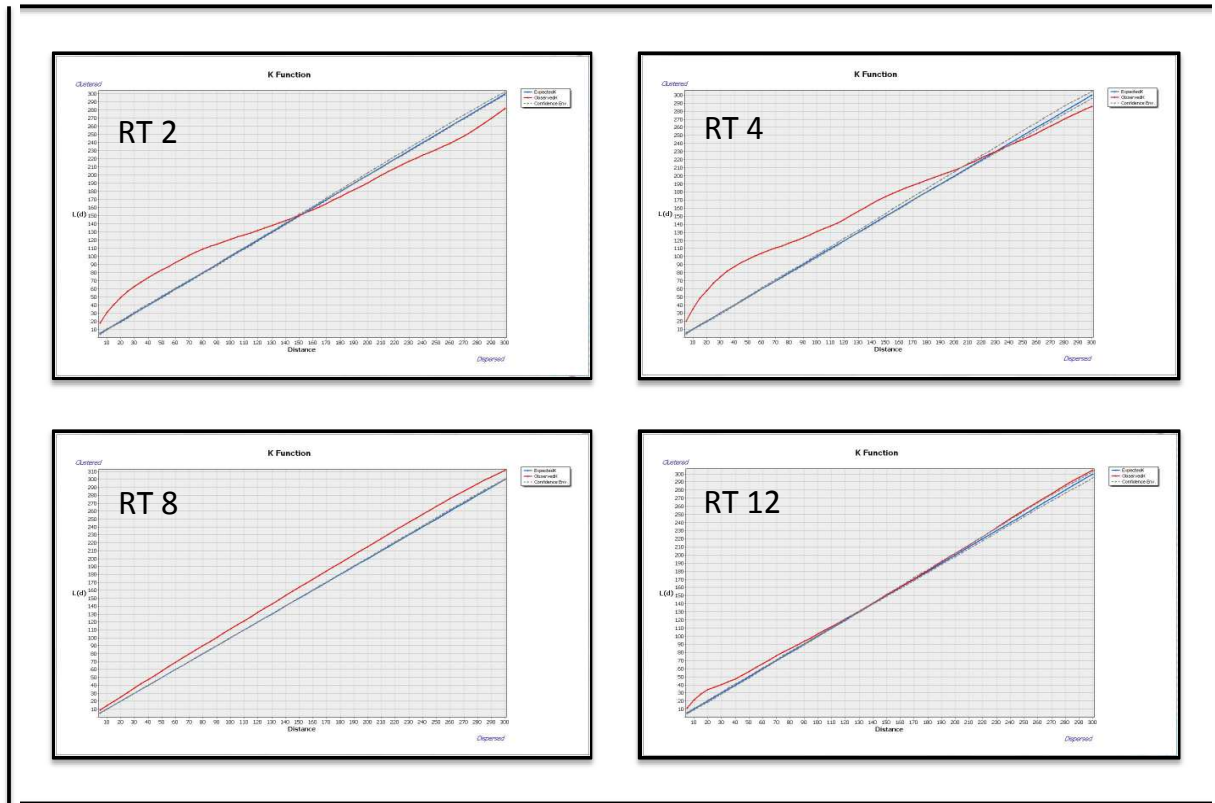


**Figure 4.3.** Cluster analysis for mica. Distance (x-axis) vs. Ripley's K (y-axis). Expected K values (blue line), observed K values (red line), and confidence interval (dotted line).

#### 4.4.2.3 Zircon ( $\text{ZrSiO}_4$ , tetragonal)

Zircon, an accessory mineral, showed significant clustering for RT 2 between 18-50  $\mu\text{m}$ , RT 4 between 5-75  $\mu\text{m}$  and RT 12 between 8-60  $\mu\text{m}$  (Fig. 4.4). RT 4 and RT 12 were most closely related and had significant clustering for a large distance span than RT 2. RT 8 did not exhibit any clustering or dispersion but rather random distribution between 25-300  $\mu\text{m}$ . RT 4 and RT 12 displayed dispersion at some distance intervals; however, the majority of zircons are found scattered in the four samples.

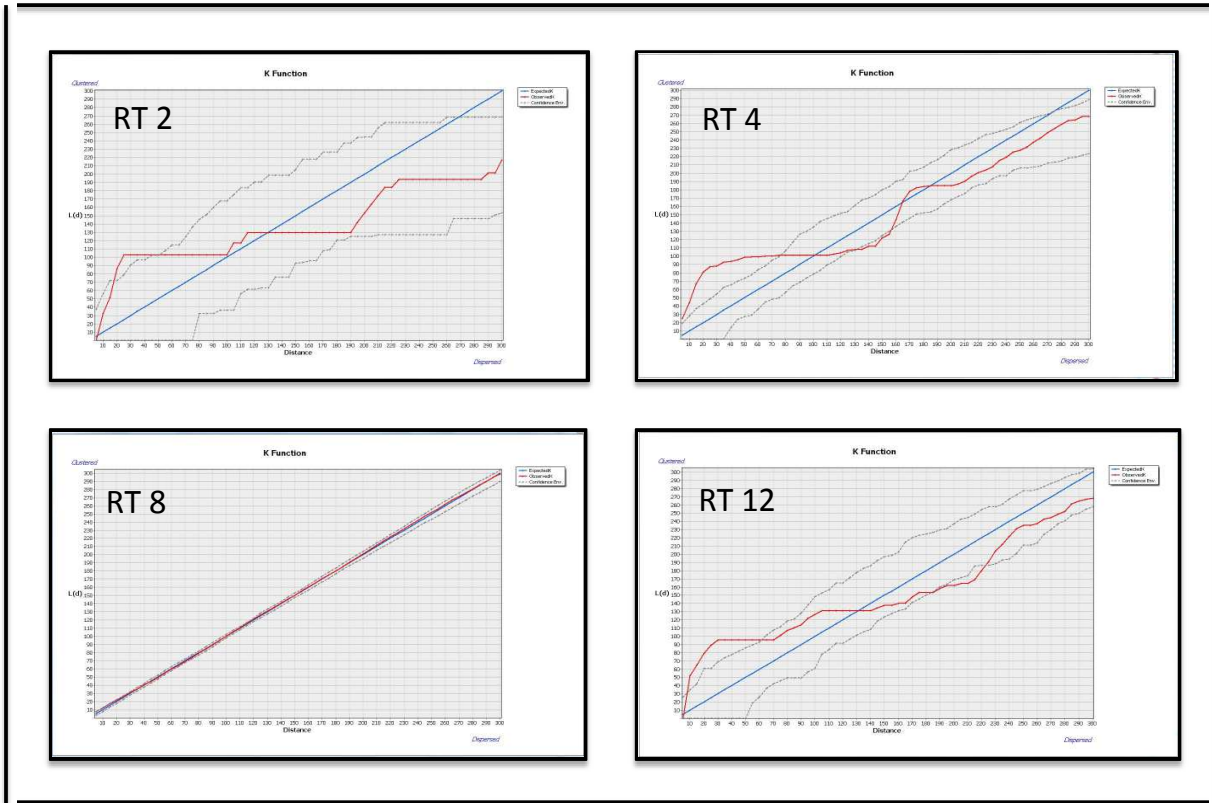


**Figure 4.4.** Cluster analysis for zircon. Distance (x-axis) vs. Ripley's K (y-axis). Expected K values (blue line), observed K values (red line), and confidence interval (dotted line).

#### 4.4.2.4 Yttrifluorite ( $\text{CaF}_2$ , isometric)

Although all four samples show statistical clustering, RT 2 stands out for its significant clustering over a large distance from 5–250  $\mu\text{m}$  (Fig. 4.5). RT 4 has clustering between 5–55  $\mu\text{m}$ , while RT 8 also shows a staggered clustering pattern between 5–60  $\mu\text{m}$ . RT 12 exhibits clustering from 5–20  $\mu\text{m}$  but as noticed in Figure 5, RT 12 begins to bend off the expected K-value line (blue) that signifies that the results are statistically significant but analytically insignificant for any points that falls in that boundary outlier. Data shows that yttrifluorite tends to occur more in clusters than random or dispersed.



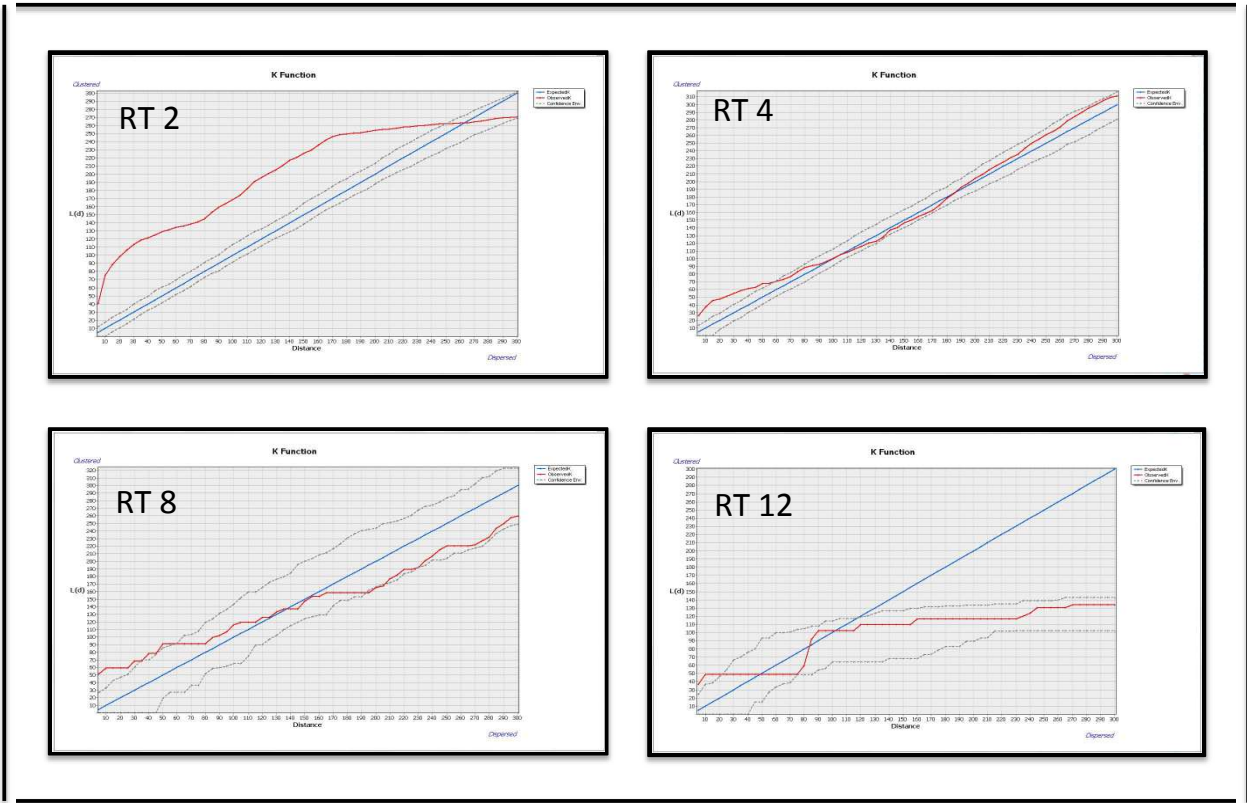


**Figure 4.5.** Cluster analysis for yttrifluorite. Distance (x-axis) vs. Ripley's K (y-axis). Expected K values (blue line), observed K values (red line), and confidence interval (dotted line).

**4.4.2.5 Cryolite ( $\text{Na}_3\text{AlF}_6$ , monoclinic)**

Cryolite has clustering for all four samples, beginning at short distances of 5  $\mu\text{m}$  up to at least 35  $\mu\text{m}$ . RT 2 ranged from 5-70  $\mu\text{m}$ , RT 8 at 5-110  $\mu\text{m}$  and RT12 had clustering up to 130  $\mu\text{m}$ . RT 2 was the only sample that exhibited dispersion at two separate distance ranges: 140-212  $\mu\text{m}$  and again at 265-300  $\mu\text{m}$ . The other three samples showed no dispersion. Though cryolite shows some clustering and dispersion, the data more strongly suggest that cryolite occur dispersed or random for samples RT 2 & 4. RT 8 and RT 12 observed K-values (red line) follow closely on the upper CI (dotted line) implying that for these samples, cryolite tends to develop in clusters.

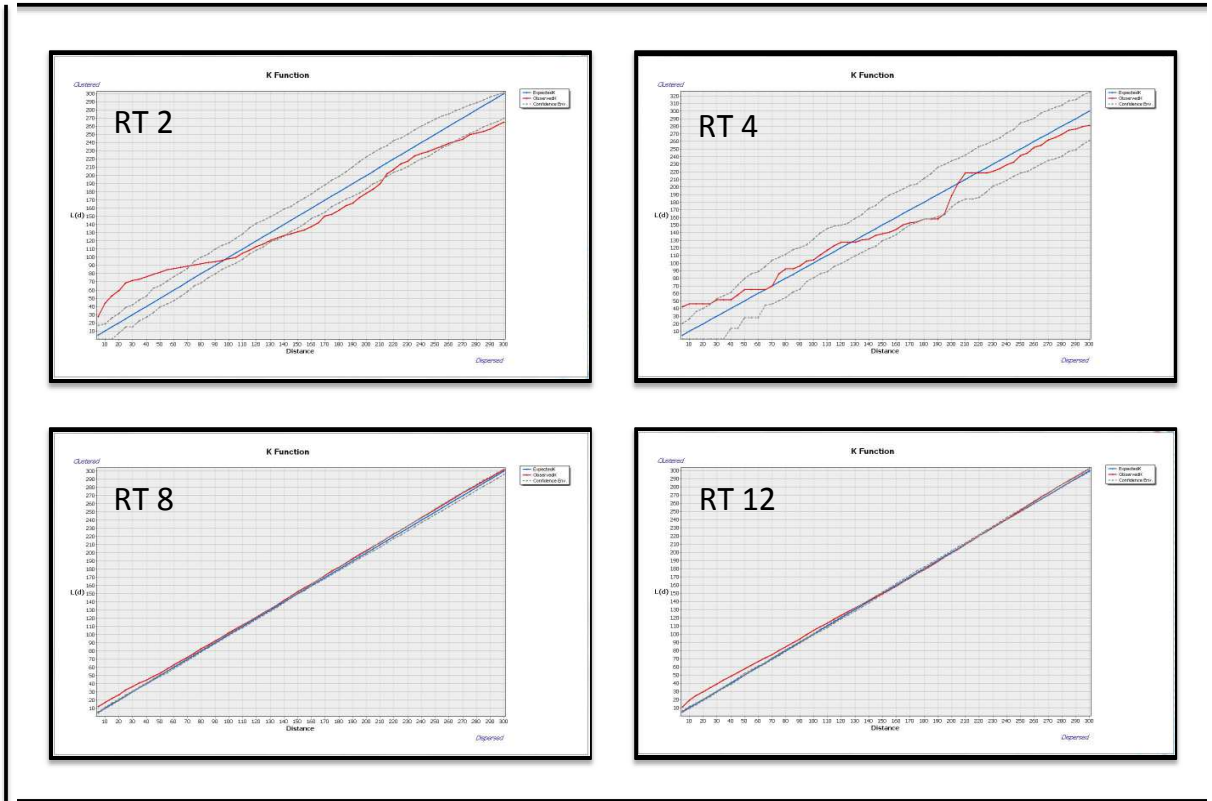


**Figure 4.6.** Cluster analysis for cryolite. Distance (x-axis) vs. Ripley's K (y-axis). Expected K values (blue line), observed K values (red line), and confidence interval (dotted line).

#### 4.4.2.6 Uraninite (UO<sub>2</sub>, isometric)

Uraninite occurs as fine disseminated grains that are found concentrated in the late magmatic fluid within the REE minerals (Gustavson, 2013). Though not abundantly, uraninite shows significant clustering in all four samples at least up to distances between 5-25  $\mu\text{m}$ ; however, the level of significance in the RT 8 and RT 12 samples are minimal compared to the other two (Fig. 7 and Table 2). Only RT 2 and RT 12 show dispersion at larger distance and both at two different intervals. RT 2 occurs dispersed between 170-198  $\mu\text{m}$  and again at 245-295  $\mu\text{m}$  while RT 12 presented at 150-172  $\mu\text{m}$  and 212-285  $\mu\text{m}$ . These graphs show that uraninite appears in clusters for shorter distances but is relatively dispersed or randomly distributed in all samples.

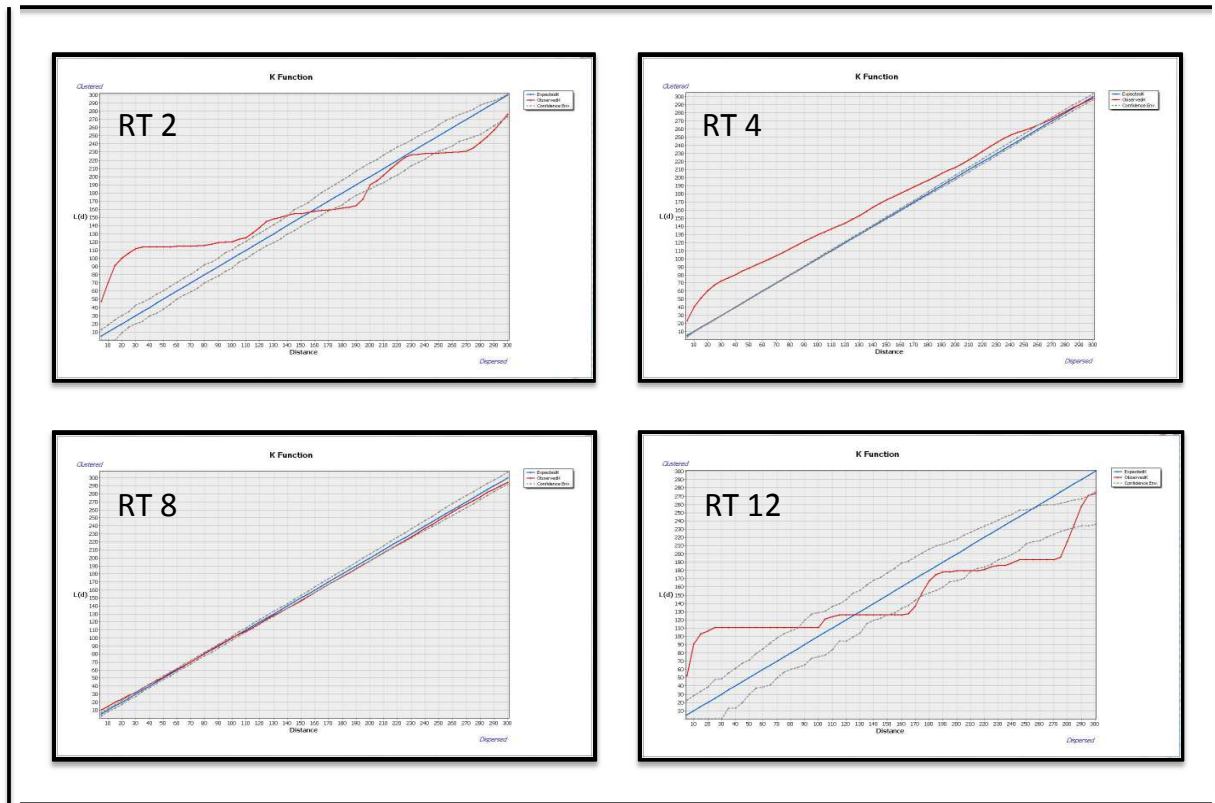


**Figure 4.7.** Cluster analysis for uraninite. Distance (x-axis) vs. Ripley's K (y-axis). Expected K values (blue line), observed K values (red line), and confidence interval (dotted line).

#### 4.4.2.7 Thorite ((Th,U) SiO<sub>4</sub>, tetragonal)

RT 2 and RT 12 show similar statistically significant clustering at distances between 5-55  $\mu\text{m}$ . RT 8 does exhibit statistically significant clustering between 70-100  $\mu\text{m}$ ; but mostly it shows clustering that follows the upper CI level from 5-140  $\mu\text{m}$  where it crosses the expected K-values (blue line) and thorite becomes randomly distributed (Fig. 8). RT 4 does not show any clustering but has random or dispersed distribution trends. Only RT 12 displays statistically significant dispersion from 260-285  $\mu\text{m}$ . Typically seen in close proximity to one another, thorite like uraninite also occurs randomly distributed for all samples despite some statistically significant clustering found in RT 2 and RT 12.

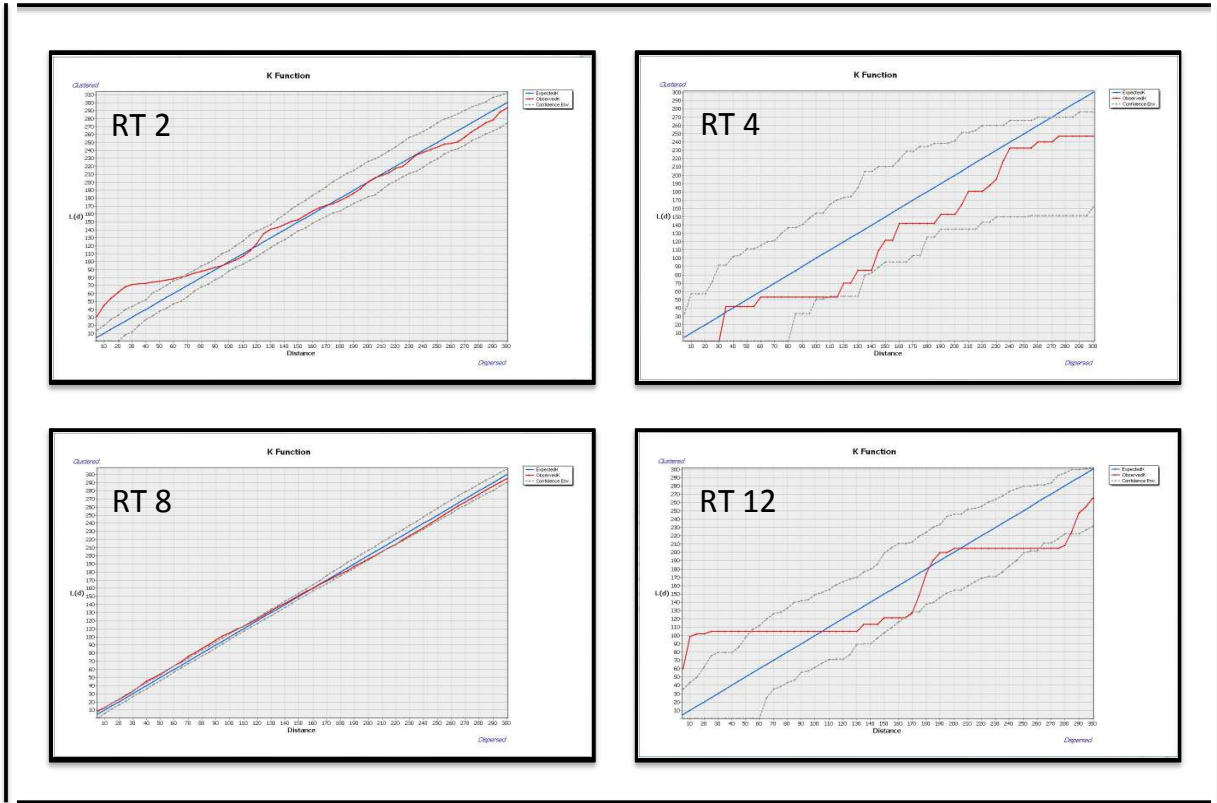


**Figure 4.8.** Cluster analysis for thorite. Distance (x-axis) vs. Ripley's K (y-axis). Expected K values (blue line), observed K values (red line), and confidence interval (dotted line).

#### 4.4.2.8 Cassiterite ( $\text{SnO}_2$ , tetragonal)

Statistically significant dispersion does not occur in any of the four samples; however, RT 4 and RT 12 have some statistically significant clustering (Fig. 9). RT 4 shows clustering between 5-40  $\mu\text{m}$  and RT 12 from 5-130  $\mu\text{m}$ . The data for cassiterite falls under 'statistical uncertainty' for RT 2 and RT 4 that has a bend in their data. RT 8 shows a random distribution for the majority of distance 20-300  $\mu\text{m}$  and RT 12 displays a similar trend at distances 150-180  $\mu\text{m}$  and 210-275  $\mu\text{m}$ .

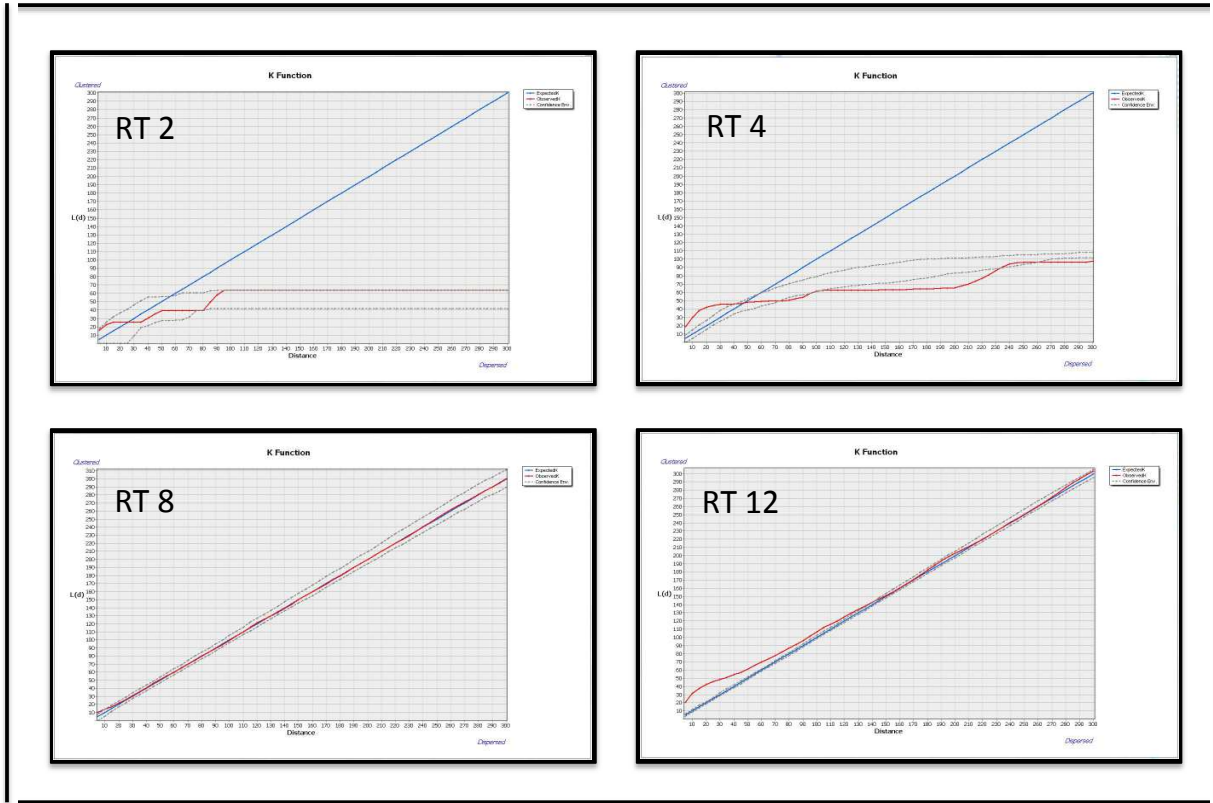


**Figure 4.9.** Cluster analysis for cassiterite. Distance (x-axis) vs. Ripley's K (y-axis). Expected K values (blue line), observed K values (red line), and confidence interval (dotted line).

#### 4.4.2.9 Columbite ( $\text{Fe}^{2+}\text{Nb}_2\text{O}_6$ , orthorhombic)

This mineral had 2 samples that show clustering at similar distances between 5-70  $\mu\text{m}$  RT 2 and RT 12 (Fig. 10). RT 2 has statistically significant clustering between 5-85  $\mu\text{m}$  and 115-165  $\mu\text{m}$ . Though not statistically significant, RT 2 does tend toward clustering from 5-200  $\mu\text{m}$  where it crosses to random and then dispersed distribution. Statistically significant dispersion occurred at large distances from 280-298  $\mu\text{m}$ . RT 4 did not display clustering at any distance but did have significant dispersion at distance between 185-238  $\mu\text{m}$  before values began to curve, rendering the remaining data invalid. The RT 8 sample is not very clear and appears to follow the expected K-values (blue line) a random distribution from 15-300  $\mu\text{m}$  where it becomes clearer that the

observed K-values follow the lower CI that relates to a dispersed distribution. Other than RT 2 that has statistically significant clustering for a large range in distance and RT 12 for a shorter range of distance other than those areas of clustering, columbite exhibits either a random or dispersed spread generally between all samples.

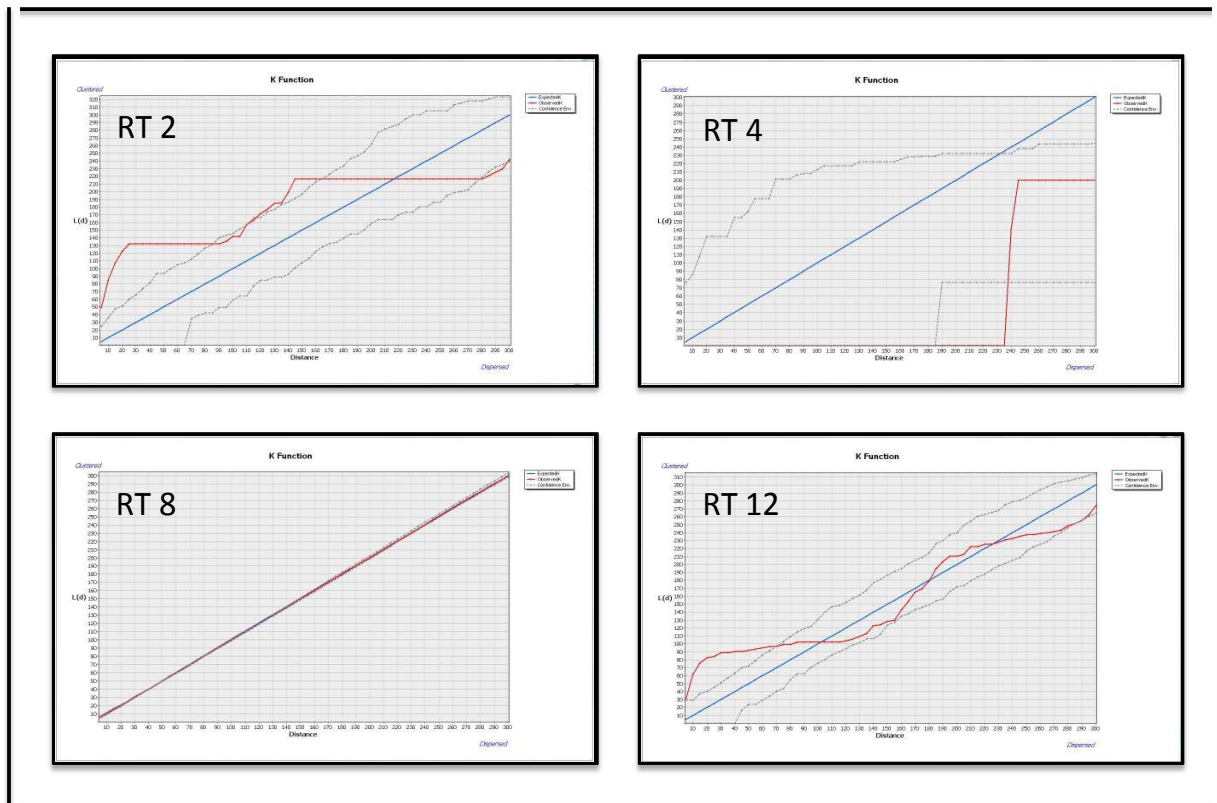


**Figure 4.10.** Cluster analysis for columbite. Distance (x-axis) vs. Ripley's K (y-axis). Expected K values (blue line), observed K values (red line), and confidence interval (dotted line).

#### **4.4.2.10 Data summary**

Table 4.2 displays a summary of all distances for nine minerals for each of the four samples, broken into three categories: statistically significant clustering, statistically significant dispersion, and random distribution. Statistically significant clustering or dispersion refers only to those areas where the observed K-values (red line) lie either above or below the confidence interval (CI). This table does not assert that these are the only areas where clustering or dispersion can or does occur. Randomly distributed implies when the observed K-values fall at or closely near the expected K-values (blue line). Where “N/A” is seen, it signifies that for that mineral in that particular sample, one of the following columns does not apply.

**Table 4.2.** Summary of spatial cluster analysis of 9 minerals showing distances at which significant clustering, significant dispersion and random distributions occur in Round Top Mountain samples (Ripley's K-function analysis).

Minerals	Statistically Significant Clustering ( $\mu\text{m}$ )				Statistically Significant Dispersion ( $\mu\text{m}$ )				Random ( $\mu\text{m}$ )			
	RT 2	RT 4	RT 8	RT 12	RT 2	RT 4	RT 8	RT 12	RT 2	RT 4	RT 8	RT 12
Magnetite	10-120	5-80	10-80	N/A	232-300	242-300	N/A	200-215	160-190	170-190	105-245	50-60 & 90-105
Mica	5-150	5-205	5-300	5-110 & 270-300	150-300	245-300	N/A	N/A	N/A	225-235	N/A	115-180
Zircon	18-45	5-75	N/A	8-60	N/A	130-155	N/A	190-225	90-140	95-105 & 165-190	25-300	125-140
Yttrifluorite	5-250	5-55	5-65	5-20	N/A	N/A	N/A	N/A	90-120 & 180-200	260-270	115-165	45-55
Cryolite	5-70	5-35	5-110	5-130	140-212 & 265-300	N/A	N/A	N/A	90-105	60-135 & 205-225	N/A	140-250
Uraninite	5-140	5-260	5-25	5-85	170-198 & 245-295	N/A	N/A	150-172 & 212-285	150-165 & 215-230	280-300	50-110	120-130
Thorite	5-65	N/A	70-100	5-55	N/A	N/A	N/A	260-285	90-120 & 150-250	32-60	140-180	100-110 & 180-205
Cassiterite	N/A	5-40	N/A	5-130	N/A	N/A	N/A	N/A	20-30	45-50	20-300	150-180 & 210-275
Columbite	5-85 & 118-162	N/A	5-15	5-70	280-298	185-238	N/A	N/A	200-230	N/A	15-300	95-105, 170-180, 220-240



## 4.5 DISCUSSION AND CONCLUSIONS

In an earlier work (Negron et al., 2019) we showed that overlaying the X-ray element maps in ArcGIS™ revealed element-mineral correlations to produce mineralogical maps. In this paper we described the use of those detailed maps to study the placement of minor and accessory minerals, relative to one another in order to understand mineral relationships at the micron-scale. Proximity and cluster analysis was performed on four mineral maps constructed using X-Ray images produced by EPMA via thin section and ArcGIS™ in order to determine point distances and construct clustering graphs.

Nine minor and accessory minerals were examined in these Round Top Mountain samples, of which yttrifluorite is of most economic importance. Yttrifluorite is either found in clusters at short distances between 5-20  $\mu\text{m}$  or randomly spread throughout 2 x 2 mm areas of the rhyolite sampled. Proximity analysis of yttrifluorite, with respect to all four RT maps, showed that the shortest distance between YF grains is 30  $\mu\text{m}$  and the largest distance is 2000  $\mu\text{m}$ . We also determined that yttrifluorite grains are found neighboring potassium feldspar and quartz grains, but also more commonly near Fe-bearing minerals, chiefly magnetite and annite mica. YF grains in close proximity to one another suggest that the YF and any other soluble minerals that lie near or conjointly, might be extractable together.

Further evaluation showed that clustering exists for all minerals; however, they do not necessarily exist in all samples. Dispersion occurs for most minerals at greater distances, between 130-300  $\mu\text{m}$ , but not for all samples. Where clustering or dispersion was absent, minerals were distributed randomly throughout the sampled area. Sites where YF and other minor or trace minerals are in close proximity suggest that they may have formed or been emplaced at the same time in this deposit. This information helps our understanding of how REE bearing

minerals relate to one another and how to potentially extract those specific target minerals together. This clustering, especially near Fe-bearing minerals which are soluble with dilute sulfuric acid, will hopefully allow the ability to yield higher extraction of HREEs due to their close proximity and their proximity to pore space that will open from the dilute sulfuric acid and subsequently the rate limiting diffusion heap leach of the deposit.

## **ACKNOWLEDGEMENTS**

The authors thank Texas Mineral Resources Corporation for providing access to proprietary technical data and samples. This project was supported by joint research contracts 26-8211-12 and 26-8211-16 between TMRC and the University of Texas at El Paso. Funds to cover the costs to publish in open access were obtained from this source. Also, we thank Dr. Ortolano and Ph.D candidate Roberto Visalli from the University of Catania for access to their X-ray Map Analyzer application.

## **References**

Anju, M., & Banerjee, D.K. (2012) Multivariate statistical analysis of heavy metals in soils of Pb-Zn mining area, India. *Environmental Monitoring and Assessment*, **184**(7), 4191-4206.

Audet, R.H. and Abegg, G.L. (1996) Geographic Information Systems: Implications for Problem Solving. *Journal of Research in Science Teaching*, **33**(1), 21-45.

[https://doi.org/10.1002/\(SICI\)1098-2736\(199601\)33:1<21::AID-TEA2>3.0.CO;2-R](https://doi.org/10.1002/(SICI)1098-2736(199601)33:1<21::AID-TEA2>3.0.CO;2-R)

Chatterjee, N. (2012) Electron Microprobe Analysis. MIT Course 12.141 Notes

Gustavson Associates (2013) NI 43-101 Preliminary Economic Assessment: Round Top Project, Sierra Blanca, Texas. [http://tmrcorp.com/news/technical\\_reports/](http://tmrcorp.com/news/technical_reports/)

Khashgerel, B., Kavalieris, I. & Hayashi, K. (2008) Mineralogy, textures, and whole-rock geochemistry of advanced argillic alteration: Hugo Dummett porphyry Cu-Au deposit, Oyu Tolgoi mineral district, Mongolia. *Mineralium Deposita*, **43**(8), 913-932. DOI 10.1007/s00126-008-0205-3

Lee, Y., Song, Y. (2007) Selecting the key research areas in nano-technology filed using technology and cluster analysis: A case study based on National R&D Programs in South Korea. *Technovation*, **27**(1-2), 57-64.

Ma, L., Sun, J., Yang, Z., Wang, L. (2015) Heavy metal contamination of agricultural soils affected by mining activities around the Ganxi River in Chenzhou, Southern China. *Environmental Monitoring and Assessment*, **187**: 731. <https://doi.org/10.1007/s10661-015-4966-8>

Mitchell, Andy. (2005) *The ESRI Guide to GIS Analysis*, **2**. ESRI Press

Negrón, L., Pingitore Jr., N.E., Gorski, D. (2016) Porosity and Permeability of Round Top Rhyolite (Texas, USA) Favor Coarse Crush Size for Rare Earth Element Heap Leach. *Minerals*, **6**(1), 16; DOI:10.3390/min6010016. <http://www.mdpi.com/2075-163X/6/1/16>

Negrón, L., Pingitore Jr., N.E., Gorski, D. (2019, in submission) ArcGIS™ and Principal Component Analysis of Probe Data to Micro-map Minerals in Round Top Rare Earth Deposit.

O'Neill, LC. (2014) REE-Be-U-F mineralization of the Round Top laccolith, Sierra Blanca peaks, Trans-Pecos Texas. MSc thesis, University of Texas at Austin.

O'Neill, L.C., Elliott, B.A., and Kyle, J.R. (2017) Mineralogy and crystallization history of a highly differentiated REE-enriched hypabyssal rhyolite: Round Top laccolith, Trans-Pecos, Texas. *Mineralogy and Petrology*, **111**, 569-592. DOI 10.1007/s00710-017-0511-5

Ortolano, G., Zappalà, L., Mazzoleni, P. (2014) X-ray Map Analyser: A new ArcGIS™® based tool for the quantitative statistical data handling of X-ray maps (Geo- and material-science applications). *Computers & Geosciences*, **72**, 49-64. <https://doi.org/10.1016/j.cageo.2014.07.006>

Pingitore Jr. N.E., Clague, J.W., and Gorski, D. (2012) Round Top Mountain (Texas, USA) a Massive, Unique Y-bearing-fluorite-hosted Heavy Rare Earth Element (HREE) Deposit. *Journal of Rare Earths*, **32**, 90-96. [https://doi.org/10.1016/S1002-0721\(14\)60037-5](https://doi.org/10.1016/S1002-0721(14)60037-5)

Pingitore Jr., N.E., Clague J.W, Gorski, D. (2018a) Remarkably consistent rare earth element grades at Round Top yttrifluorite deposit. *Advances in Materials Physics and Chemistry, Special Issue: Rare Earth Elements*, 8(1), 1-14. DOI: 10.4236/ampc.2018.81001

Pingitore Jr., N.E., Piranian, M., Negrón, L., Gorski, D. (2018b) Microprobe Mapping of Rare Earth Element Distribution in Round Top Yttrifluorite Deposit. *Advances in Materials Physics and Chemistry, Special Issue: Rare Earth Elements*, **8**(1), 15-31. DOI: 10.4236/ampc.2018.81002 <https://doi.org/10.4236/ampc.2018.81002>

Price, J.G, Rubin J.N., Henry, C.D., Pinkston, T.L., Tweedy, S.W., Koppenaar, D.W. (1990) Rare-metal enriched peraluminous rhyolites in a continental arc, Sierra Blanca area, Trans-Pecos Texas; chemical modification by vapor-phase crystallization. *GSA Special Papers* 246, 103-120. <http://dx.doi.org/10.1130/SPE246-p103>

Price, M.H. (2016) *Mastering ArcGIS™*. McGraw Hill Education. Seventh Edition.

Rubin, J.N., Price, J.G., Henry, C.D. and Koppenaar, D.W. (1987) Cryolite-Bearing and Rare Metal-Enriched Rhyolite, Sierra Blanca Peaks, Hudspeth County, Texas. *American Mineralogist*, **72**, 1122-1130

Shannon, W.M (1986) Lithogeochemical characterization of intrusive rocks comprising the Quitman-Sierra Blanca igneous complex, Hudspeth County, Texas. MSc thesis, University of Texas at El Paso.

Sprague, K., de Kemp, E., Wong, W., McGaughey, J., Perron, G., Tucker, B. (2006) Spatial targeting using queries in a 3-D GIS environment with application to mineral exploration.

*Computers & Geosciences*, **32** (3), 396-418. <https://doi.org/10.1016/j.cageo.2005.07.008>

Yttrofluorite. Mindat (2019) <https://www.mindat.org/min-4371.html>

Zhang, L., Lui, X., Janssens, F., Liang, L., Glänzel, W. (2010) Subject clustering analysis based on ISI category classification. *Journal of Informetrics*, **4**(2), 185-193.

## Curriculum Vita

Lorraine M. Negrón earned her Bachelor of Science degree in Earth Science with a minor in Environmental Science from The University of Michigan in 2010. She joined UTEP in 2011 pursuing a Masters then transitioned into the doctoral program in Geological Sciences.

Dr. Negrón was the recipient of the Master's Graduate Student of the Year award in 2012 at UTEP. In 2013 she was the recipient of a NSF fellowship, GK-12 Graduate Fellow. She received the Vernon G. Rowling and Joy Hunt Endowed Scholarship Fund in Geology in 2014 and 2018.

Dr. Negrón has presented her research at several meetings including 2012 Geological Society of America on "U-series Chronology of volcanoes in the Central Kenya Peralkaline Province, East African Rift". In 2013 American Geophysical Union Fall Meeting on "Fluorescein Dye Penetration in Round Top Rhyolite (Hudspeth County, Texas, USA) to Reveal Micro-Permeability and Optimize Grain Size for Heavy REE Heap Leach". Then in 2015 Society for Environmental Geochemistry and Health on "Gastrointestinal bioavailability of select metals in Round Top Mountain rhyolite". She has published work that appears in the journals *Minerals* and *Advances in Materials Physics and Chemistry*. She has forthcoming articles that are also to appear in *Advances in Materials Physics and Chemistry*.

While pursuing her degree, Dr. Negrón worked as a teaching assistant for the Department of Geological Sciences, a tutor for El Paso Community College, adult and child swim instructor at the University of Texas Recreational Center, and a wellsite geologist for Terra Guidance.

Permanent address: 1410 East Easter Ave  
Centennial, CO 80122

This dissertation was typed by Lorraine M. Negrón.